



Variability and upward trend in the kinetic energy of western boundary currents over the last century: impacts from barystatic and dynamic sea level change

Tal Ezer¹ · Sönke Dangendorf¹

Received: 12 November 2020 / Accepted: 6 May 2021 / Published online: 15 May 2021
© The Author(s), under exclusive licence to Springer-Verlag GmbH Germany, part of Springer Nature 2021

Abstract

Global sea level reconstruction (RecSL) for 1900–2015 was used to estimate the variations in oceanic kinetic energy (OKE) and compare OKE with changes in wind patterns and wind kinetic energy (WKE); the comparison was done for each latitude and for 5 western boundary currents (WBCs). Two contributors to variability in sea level were analyzed: gravitational, rotational and deformational effects (GRD) related to changes in water masses (barystatic sea level change), and changes in the steric dynamic sea level (SDSL), associated with changes in wind, steric sea level and ocean circulation. GRD changes were responsible for latitudinal multidecadal variations with time scale of ~60 to 80 years, while SDSL changes were responsible for interannual and decadal variability, and together with the Greenland ice melt, to sea level acceleration since the 1960s. Regional changes near WBCs show a coherent upward trend in OKE (+24% ± 3 increase per century), while trends in WKE over the same regions changed widely from -11% (decrease) over the Gulf Stream region to +28% (increase) over the Brazil Current region. Low frequency oscillations of wind and oceanic kinetic energy are correlated in some WBCs (e.g., $R=0.5$ in the Kuroshio region) but not in others (e.g., $R=-0.05$ in the Gulf Stream region). The study suggests that several forcing mechanisms contribute to the increased OKE, they include an increased wind-stress curl over subtropical gyres, local changes in wind patterns that impact some WBCs, and large uneven warming near WBCs that increased sea level gradients and thus intensified OKE.

Keywords Sea-level change · Western boundary currents · Climate change · Barystatic sea-level · Oceanic kinetic energy

1 Introduction

While global sea level rise (SLR) over the past century has been accelerating (Church and White 2006, 2011; Merrifield et al. 2009; Jevrejeva et al. 2008; Hay et al. 2015; Dangendorf et al. 2014, 2017, 2019), SLR has considerable decadal and multi-decadal variations and large spatial regional differences. With climatic changes, the relative contribution to SLR from different sources is changing over time, so for example, in recent decades changes in water masses (barystatic sea level change) due to land-ice melting and hydrological processes increased its relative contribution to SLR compared with contribution from changes in salinity and

temperature (steric sea level). Each of the contributors to SLR has different variations in space and time when considering the total budget of SLR (Frederikse et al. 2020). In addition, there are climatic changes in the dynamics of the atmosphere and the ocean circulation, and these changes are linked to climatic changes in sea surface height (SSH) and sea surface temperature (SST) over the oceans. Cai (2006) for example, linked Antarctic ozone depletion with intensification of the winds over the Southern Ocean and Dangendorf et al. (2019) linked the intensification of winds there with accelerated global SLR after the 1960s.

When considering the role of ocean dynamics in climate change, Western Boundary Currents (WBCs) play a critical role. The WBCs are the intense wind-driven currents at the western edge of subtropical gyres- these warm currents play an important role in the meridional heat transports of the oceans and the mass and heat balance of the earth system. Recent studies, using sea surface temperature data, atmospheric reanalysis data and climate models, indicate that

✉ Tal Ezer
tezer@odu.edu

¹ Center for Coastal Physical Oceanography, Old Dominion University, 4111 Monarch Way, Norfolk, VA 23508, USA

with global warming, WBCs had intensified and potentially shifted their path (Wu et al. 2012; Yang et al. 2016). These studies suggested that the causes for the changes in WBCs are poleward shift and intensification in zonal winds and increased SST, but these studies did not consider the impact of barostatic sea level changes on ocean dynamics. There are considerable differences in the response of individual WBCs to global warming (Sen Gupta et al. 2021) due to local and large-scale effects, such as impact of local topography or basin scale climate modes (Han et al. 2019). Using ensemble of climate model projections, Chen et al. (2019), for example, tried to explain why global warming would intensify the Kuroshio but weaken the Gulf Stream. Unlike most WBCs which have been projected to intensify under warmer climate, the Gulf Stream is closely linked with variations in the Atlantic Meridional Overturning Circulation, AMOC (Bryden et al. 2005; McCarthy et al. 2012; Sallenger et al. 2012; Blaker et al. 2014; Roberts et al. 2014; Ezer 2015; Rahmstorf et al. 2015; Caesar et al. 2018; Smeed et al. 2018; Little et al. 2019), thus a weakening of AMOC under warming conditions may slowdown the Gulf Stream as well (Ezer et al. 2013; Ezer 2015; Dong et al. 2019; Zhang et al. 2020). While some studies suggested that the Gulf Stream was quite stable over the past few decades, and that the downward trend is too small to detect from existing direct observations (Rossby et al. 2014), recent reconstruction of the Florida Current (FC) using sea level data did show statistically significant weakening of the FC over the last century (Piecuch 2020). Furthermore, a recent study found the fingerprint of an AMOC slowdown even in changes in salinity obtained from observations and models (Zhu and Liu 2020).

Very few direct, long-term, observations of WBCs flows exist, an exception is the cable measurement across the Florida Strait of the Florida Current (FC) transport since 1982 (Baringer and Larsen 2001; Meinen et al. 2010). Indirect monitoring of flow variations can be obtained for example from the gradients of SSH across WBCs (assuming geostrophic balance) using sea level data from satellite altimeters over a few decades or reconstructed sea level over longer periods. Ezer and Dangendorf (2020), for example, demonstrated the ability of reconstructed sea level to capture decadal variations in the flow of the Gulf Stream, which were compared with observations of the FC; they showed that variability on time scales longer than ~5 years are well represented in the reconstructed sea level. The current study is a follow up and expansion of the study of Ezer and Dangendorf (2020), using similar methods to assess flows of 5 WBCs: the Gulf Stream (GS) in the North Atlantic Ocean, the Kuroshio Current (KC) in the North Pacific Ocean, the Brazil Current (BC) in the South Atlantic Ocean, the Agulhas Currents (AGC) in the southern Indian Ocean and the East Australian Current (EAC) in the South Pacific Ocean. In all these WBCs there are large contrasts between

warmer subtropical waters (with higher SSH) on their equatorward side and colder waters (with lower SSH) on their poleward side. Interannual to long-term changes have been observed and modeled in these WBCs, for example in the GS (Greatbatch et al. 1991; Taylor and Stephens 1998; Ezer 1999, 2001, 2015, Dong et al. 2019; Andres et al. 2020; Ezer and Dangendorf 2020), in the KC (Mizuno and White 1983; Deser et al. 1999) in the BC (Goni et al. 2011) in the AGC (Lutjeharms 2006; Beal and Elipot 2016) and in the EAC (Ridgway 2007). Note however, that the WBCs in the northern hemisphere (GS and KC) have been observed and studied much more extensively than the other currents—the GS in particular has been investigated for the longest time (Montgomery 1938; Stommel 1965; Blaha 1984) and is the only WBCs with continuous directly observed monitoring of its transport (Baringer and Larsen 2001; Meinen et al. 2010). Significant global coverage of WBCs from satellite altimetry started in the early 1990s and monitoring AMOC started only in the early 2000s (McCarthy et al. 2012). Therefore, to study global changes over more than a century one must rely on reconstructed sea level which combines altimeter data and tide gauge data. Various global reconstructed sea level methods have been developed (Church et al. 2011; Compo et al. 2011; Calafat et al. 2014; Hamlington et al. 2014; Hay et al. 2015; Dangendorf et al. 2019); here the hybrid reconstruction of Dangendorf et al. (2019) is used. This monthly global reconstruction for 1900–2015 at $1^\circ \times 1^\circ$ resolution excludes land motion and seasonal variations and was previously used for example by Gehrels et al. (2020) in studies of past sea-level hotspots and by Ezer and Dangendorf (2020) in studies of long-term variability in the GS. Here, the reconstructed sea level is separated into two components, the barostatic sea level change and the dynamic sea level change (see details in the next section).

The main motivation behind the study is to explore the changes in WBCs. Several studies, using data and models, suggested that WBCs have been intensified as the climate got warmer (Deser et al. 1999; Ridgway 2007; Goni et al. 2011; Wu et al. 2012; Yang et al. 2016), attributing the WBCs changes primarily to intensification and shift in wind patterns, especially in the southern hemisphere (Cai 2006). However, other studies suggest that WBCs (the Agulhas Current in particular) are not strengthening, but broadening due to increased eddy activity (Beal and Elipot 2016), and some studies suggest that sea surface warming and not wind is responsible for the intensification of WBCs (the Kuroshio Current in particular; Chen et al. 2019). For example recent research (Martínez-Moreno et al. 2021), suggested that increased ocean eddy activity near WBCs regions since the 1990s may be the main cause of global increase in OKE. There are thus clear differences between the different WBCs that are not fully explored yet. From the trend in globally averaged oceanic kinetic energy, Hu et al. (2020) inferred

the existence of substantial acceleration in ocean circulation since the early 1990s; they found that the most pronounced intensification of ocean currents was in tropical regions and in depth, not in surface WBCs. In our study we will also use kinetic energy as a measure of the strength of ocean currents, though geostrophic calculations can only apply to surface flows in latitudes a few degrees away from the equator. While Hu et al. (2020) analyzed data and models since the 1960s, during a period of increased global wind speed, the longer reconstruction data used here since 1900 allows us to compare recent kinetic energy to values going back to the beginning of the twentieth century.

An open question is how would ice melt contribute to changes in ocean dynamics? If for example, barystatic sea level increases in subtropical gyres and decreases towards the poles, this may intensify WBCs. Recent studies on the role of water masses in the SLR budget (e.g., Frederikse et al. 2020) motivated us to further investigate their role on ocean dynamics. Because large water mass changes due to land-ice melt and their accompanied spatial sea level gradients through GRD effects are most pronounced in high latitudes, our spatial and temporal analysis is focused first on latitudinal averages and then on regional changes near 5 WBCs. The goal is to study how changes in the intensity of ocean currents are linked with changes in wind and sea level (both, barystatic and steric changes), and to assess those links and variability on both, regional and global scales.

The paper is organized as follows: the data and the analysis methods are described in Sect. 2, then in Sects. 3 the results are described, first for latitudinal variations then for regional variations near WBCs, finally, in Sect. 4, summary and conclusions are offered.

2 Data sources and analysis methods

The monthly global reconstructed sea level (RecSL) on a (1° × 1°) grid for 1900–2015 was developed by Dangendorf et al. (2019) and previously analyzed in several recent studies (Ezer and Dangendorf 2020; Frederikse et al. 2020; Gehrels et al. 2020). This reconstruction is based on combination of 479 tide gauge records, satellite altimeter data, and several geophysical ancillary datasets of contributing processes such as glacial isostatic adjustment (GIA), GRD effects and ocean models. The hybrid approach combines a Kalman Smoother technique (Hay et al. 2015) with optimal interpolation and empirical orthogonal functions, EOF (Calafat et al. 2014), taking advantage of the spatial pattern of global altimeter data and the long but unevenly spaced tide gauge records. The GIA component and the annual cycle were removed from RecSL. While most studies using global reconstructed sea level focus on sea level rise itself, Ezer and Dangendorf (2020) also show the usefulness of

the RecSL for studies of regional ocean dynamics in the Gulf Stream region, so here we extend the analysis to other subregions and provide averages over 5 regions near WBCs. Average properties along each latitude are also calculated to capture the variations associated with ice melt in high latitudes. The total RecSL is divided into two components (for details see Frederikse et al. 2020), the sea level component of GRD effects associated with barystatic mass changes (i.e., glaciers, ice-sheets and natural/anthropogenic land water storage) and the remaining is the contribution of sterodynamic sea level (SDSL). The different sea level components and definitions are described in detail by Gregory et al. (2019). The SDSL includes impacts from wind, atmospheric pressure, ocean temperature and salinity, ocean currents, and basin-scale waves and climate modes (Han et al. 2019). The purpose here was not to investigate the global SLR balance as done in Frederikse et al. (2020), but to explore the regional differences between the impact of GRD change and SDSL change with respect to ocean circulation changes in WBCs. It is noted that local spatiotemporal variations in temperature, while not directly analyzed, are closely linked with variations in sea level (Martínez-Moreno et al. 2021) due to the thermostatic effect, and thus linked with changes in geostrophic velocity as described below.

From the sea level $h(x,y,t)$ in RecSL and its change in x and y ($\Delta h/\Delta x$, $\Delta h/\Delta y$) an estimated surface geostrophic currents (U_g , V_g) can be made and from them, the oceanic kinetic energy (*OKE*, per unit mass) and relative vorticity (*VOR*) can be calculated by,

$$U_g(x,y,t) = -\frac{g}{f} \frac{\Delta h}{\Delta y}, \quad V_g(x,y,t) = \frac{g}{f} \frac{\Delta h}{\Delta x} \quad (1a, b)$$

$$OKE(x,y,t) = \frac{1}{2} (U_g^2 + V_g^2), \quad VOR(x,y,t) = \left(\frac{\Delta V_g}{\Delta x} - \frac{\Delta U_g}{\Delta y} \right), \quad (2a, b)$$

where g is the gravity constant, $f(y)$ is the Coriolis parameter and Δx , Δy , are 1° longitude or latitude. Since the Coriolis parameter is zero near the equator, geostrophic calculations are not calculated in a band ± 5° from the equator and instead values outside this zone are used; results are presented only for regions at least 10° away from the equator. For wind velocity (U_w , V_w), wind kinetic energy (*WKE*) and wind Curl (*CUR*) can be calculated by,

$$WKE(x,y,t) = \frac{1}{2} (U_w^2 + V_w^2), \quad CUR(x,y,t) = \left(\frac{\Delta V_w}{\Delta x} - \frac{\Delta U_w}{\Delta y} \right), \quad (3a, b)$$

were the units used here for kinetic energy are m²/s² and for *VOR* and *CUR* are (m/s)/deg. Oceanic relative vorticity is calculated to indicate horizontal rotation and strength of oceanic gyres and eddies. Wind stress curl can be linked to meridional oceanic transports in subtropical gyres though

the Sverdrup balance (Wunsch and Roemmich 1985). Since geostrophic velocities obtained in (1) from RecSL are expected to be underestimated due to the coarse resolution of the reconstruction, they need validation by independent data. Such examination was previously conducted for one region, the Gulf Stream, in the study of Ezer and Dangendorf (2020). They showed that flow variability on time scales longer than ~ 5 years can be captured quite well by the RecSL data (and calculations like in Eq. 1), as shown by comparisons with observations of the Florida Current and the Atlantic Meridional Overturning Circulation (AMOC). Unfortunately, there are no continuous long observations of the other WBCs for similar validation. The properties in (2) and (3) are averaged either over each latitude or over subregions near WBCs. The wind data used here is from a global reanalysis using ensemble Kalman Filter of observations as described in Compo et al. (2011). Here only wind velocity data for 1900–2015 on a ($1^\circ \times 1^\circ$) grid are used (on the same grid as the RecSL data).

Since the RecSL data is most useful for looking at long-term variability and trends, to filter out high-frequency oscillations, ensemble empirical mode decomposition (EEMD, though the term EMD is used hereafter) is applied (Huang et al. 1998; Wu et al. 2007; Wu and Huang 2009). The EMD decomposed a time series into oscillating modes and a (non-linear) trend, so summing up low-frequency modes and the trend is equivalent to a low-pass filter. The EMD has been used in numerous sea level studies (Ezer and Corlett 2012; Ezer et al. 2013; Ezer 2015), and in Ezer and Dangendorf (2020) the EMD analysis was compared with wavelet analysis for the same RecSL data used here. To calculate significance levels of correlations between low frequency EMD modes, the effective degrees of freedom was estimated following Thiebaut and Zwiers (1984). Therefore, for the 116-year long monthly record of RecSL, correlation of $R > 0.1$ provides over 95% confidence level in the correlation, but for low frequency EMD modes with typical time scales of ~ 5 to 10 years there is lower degrees of freedom so that correlation of $R > 0.45$ is estimated to be needed to have the same 95% confidence level.

3 Results

3.1 Latitudinal variations and trends

3.1.1 Barystatic GRD effects versus sterodynamic sea level

The mean sea level rise (SLR) rates for two periods, 1900–1960 and 1960–2015, are shown in Fig. 1a, b, respectively. The barystatic (GRD) contribution (Fig. 1c, d) is compared with the dynamic (SDSL) contribution (Fig. 1e, f). The largest changes, in both components of sea level is

seen along the coasts of Greenland, where GRD has dropped due to the gravitational effects of ice loss (Frederikse et al. 2020), while the SDSL has risen. The two components do not completely balance each other, creating differences between the Labrador Sea west of Greenland and the sub-polar region east of Greenland. However, there is great uncertainty in the glacial isostatic adjustment (GIA) in this region that may have affected the accuracy of the RecSL reconstruction there, so these changes should be taken very cautiously. After 1960, changes in GRD start to show up near the western Antarctic coast (Fig. 1d); lack of a signal near Antarctica prior to the 1960s is partly due to the lack of data on Antarctic ice melt that could have been entered into the RecSL analysis. The impact of SDSL (Fig. 1e–f) is more pronounced after the 1960s, and in regions with strong oceanic currents such as WBCs, near the Pacific Equatorial Currents, and in the Antarctic Circumpolar Current (ACC); the latter is an area of large recent change in the position and intensity of Southern Hemispheric westerly winds (Cai 2006; Dangendorf et al. 2019). The increase in SLR due to SDSL in the Indian Ocean (Fig. 1e vs. f) may be due to increased steric sea level there (see extended data Fig. 4 in Frederikse et al. 2020).

Since the GRD effects originate primarily from high-latitude regions, it is useful to look at latitudinal variations in sea level, so Fig. 2 shows the latitude-mean sea level rise as a function of time. There is a clear distinction between the water mass GRD impact (Fig. 2b) and the sterodynamic SDSL impact (Fig. 2c). The impact of GRD has long time scale with apparent cyclic behavior with period of ~ 60 to 80 years with fast sea level rise in the 1930s–1940s and after 2000 and slower sea level rise in the 1970s. This pattern resembles the 60-year oscillation cycle shown by Chambers et al. (2012), which was suggested by some studies to be related to the 60-year oscillations of the Atlantic Multidecadal Oscillation (AMO; Enfield et al. 2001). Ezer and Dangendorf (2020) for example, found that variations with time scale of ~ 60 -year period in AMO are coherent with similar variations in the Gulf Stream strength which represents contribution from regional GRD (see their Fig. 10), but cause and effect between AMO and GRD were not established. Frederikse et al. (2020) suggested that this long cycle may not necessarily be a natural oscillation. They show that the fast SLR in the 1940s due to mass loss from Greenland ice sheet and glaciers was slowed down in the 1970s due to increased water impoundment (dam constructions peaked in the 1970s; Chao et al. 2008), which followed by recent decades of accelerated SLR due to combination of increased ice-mass loss and thermal expansion. Studies also show that anthropogenic forcing dominated global mean SLR after the 1970s (Slangen et al. 2016). A decreased in sea level due to GRD impact on gravity is limited to areas north of $\sim 60^\circ$ N. It is noted however, that there are limited tide gauges

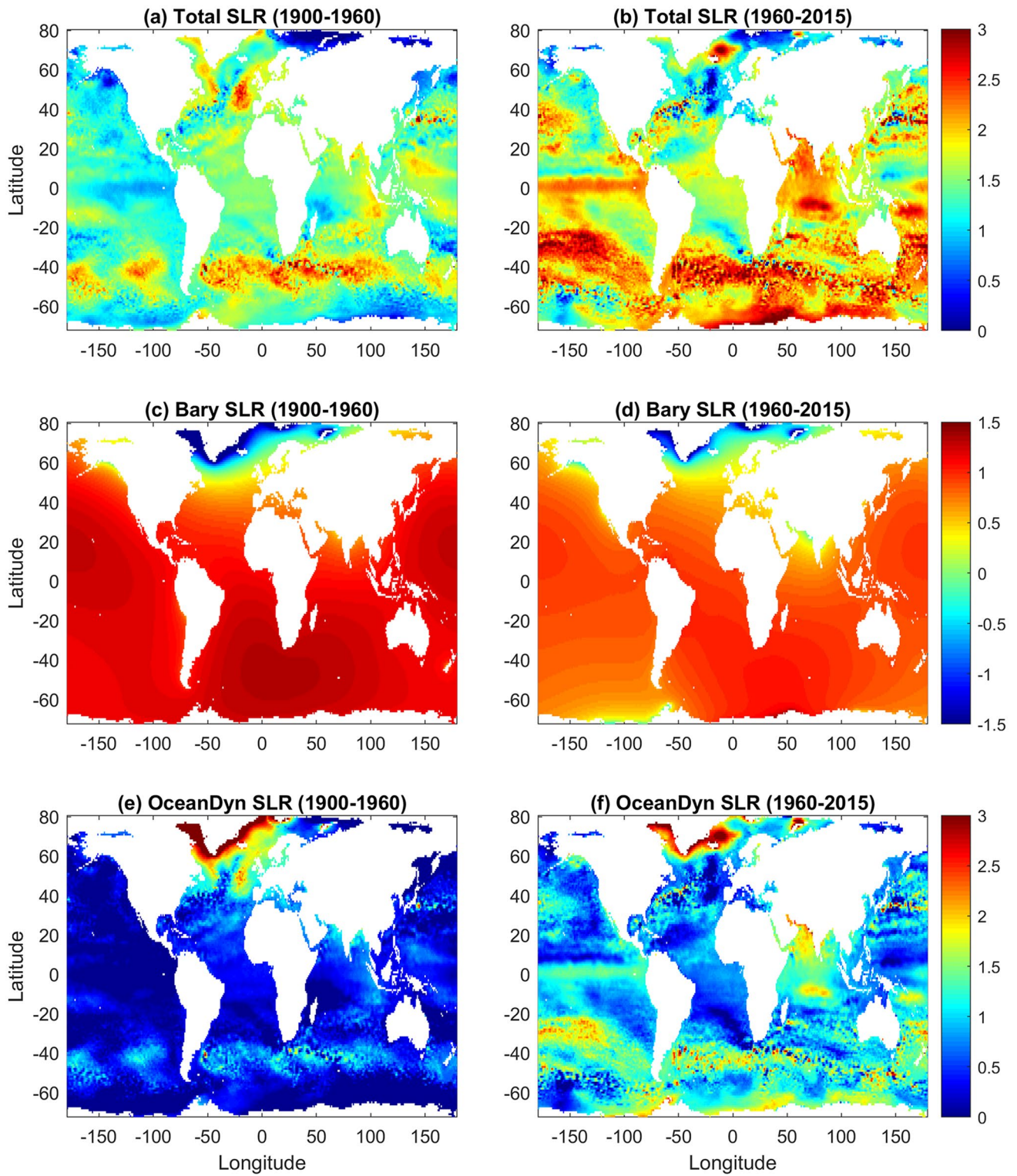


Fig. 1 Mean sea level rise (SLR in mm/year) before 1960 (left panels) and after 1960 (right panels) from the sea level reconstruction 1900–2015. From top to bottom are the total SLR, the barystatic contribution due to water masses (GRD) and the sterodynamic contribu-

tion (SDSL), respectively. The large trends near Greenland could be due to uncertainties in the GIA component. Note that the color scale for the middle panels is different than the rest

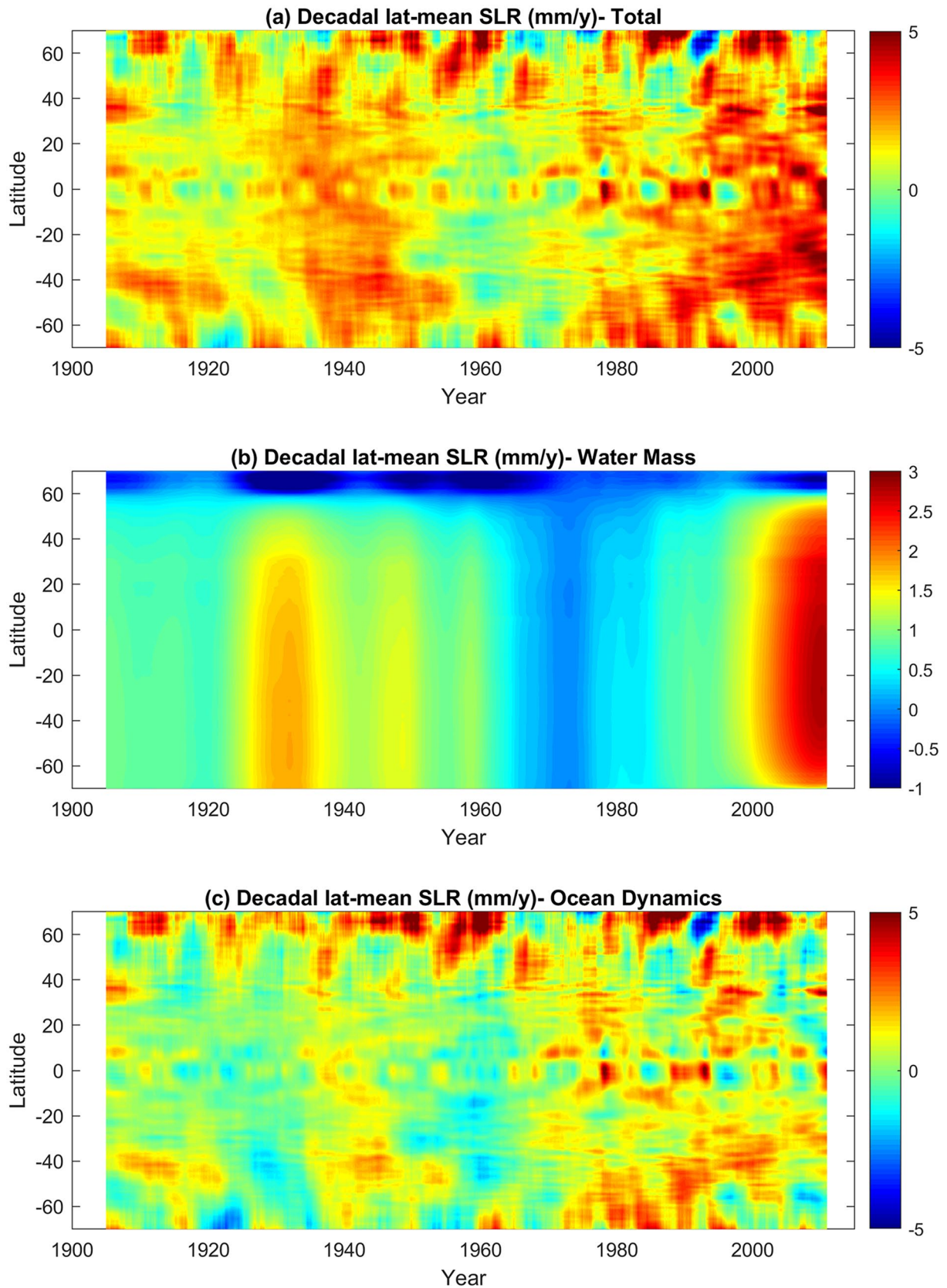


Fig. 2 Latitudinal mean decadal SLR rates (calculated from overlapping 10-year segments) for: **a** total sea level (RecSL), **b** barystatic sea level (GRD), and **c** dynamics sea level (SDSL)

observations in high latitudes, so RecSL may have greater uncertainties there. On the other hand, the SDSL has large interannual variability and much more small-scale spatial variations than the GRD does, since several sources can contribute to variations in SDSL, such as changes in temperature, salinity wind and ocean currents. To assess the relative contribution to sea level rise from GRD and SDSL, time series of latitudinally averaged sea level is shown for selected latitudes from 70° N to 70° S (Fig. 3). The only shown latitude where GRD impact is dropping sea level is at 70° N (near Greenland; top-left panel of Fig. 3) where the total sea level rise follows the SDSL. At 70° S (bottom-right panel of Fig. 3) GRD impact starts flattening after the 1960s due to Antarctic mass loss (as seen in Fig. 1d) and accompanied reduced gravity pull. Note also the high-frequency variability in high latitudes (70° N, 50° N and 70° S); in these regions lack of tide gauge data and uncertainty in GIA may contribute to the noise seen there, but it is also possible that there are some real dynamic variability near coasts with significant ice melt or atmospheric variability. Piecuch et al. (2019) for example, observed large high-frequency sea level variability near high-latitude coasts that could be associated with shelf response to atmospheric variability. In most latitudes away from sub polar regions (30° N–50° S) the total sea level rise follows the GRD until the 1960s (i.e., only small contribution from SDSL), but after the 1960s significant acceleration in sea level seems to be contributed by SDSL, as shown also in Fig. 2c. This dynamic response could be due to recent changes in wind, thermal structure, and ocean currents, which will be evaluated next.

3.1.2 Wind and oceanic kinetic energy

Changes in total oceanic kinetic energy (OKE; Eq. 2) for each latitude are shown in Fig. 4 (these are changes relative to 1900). Except an unusual drop in OKE at 70°S before 1920 (probably due to lack of data at that period), there is a general trend of increased OKE everywhere. The high frequency variations in OKE are likely due to small-scale variations in ocean dynamics, as seen in Fig. 2. What is driving the variability and trends of the OKE seen in Fig. 4? In addition to internal ocean dynamics, variations in the wind stress can cause changes in the Ekman transports and variations in wind stress curl can cause changes in the Sverdrup transport (note however, that the Sverdrup balance may be in question for some parts of the oceans, as shown for example by Wunsch and Roemmich 1985). Since wind is mostly zonal, wind stress curl (Eq. 3) is largely latitudinally dependent. In Fig. 5, low frequency variations in wind stress curl are shown with the OKE at several latitudes. The low pass filtered latitudinal means are the sum of the low frequency EMD modes plus the EMD trend. Low latitude regions (10° N and 10° S), where geostrophic velocities are

less accurate, were omitted. Given the degrees of freedom in the EMD modes (see Ezer and Dangendorf 2020), 95% confidence level is obtained for correlations greater than ~ 0.45 . In high latitudes negative CUR-OKE correlations are seen (50° N and 70° S), but in latitudes between 50° S and 30° S, increased wind stress curl is accompanied by increased OKE with correlations of 0.49–0.65 (these correlations include the trends). Since subtropical gyres are the regions of the world oceans where the Sverdrup balance is more likely to hold, the result here is reasonable, while in high latitudes other factors such as ice melt and temperature change may play a larger role. It should be noted though that interpretation of latitudinal averaged values is limited, because wind stress curl is mostly a basin-scale driver of circulation, so local calculations of CUR may only represent part of the variability. Therefore, a closer look of the wind influence on regional scales will be evaluated in the next section.

Figure 6 summarizes the trends in the wind (WKE and CUR) and in the ocean (OKE and VOR). Trends in wind kinetic energy (Fig. 6a) do not seem to resemble the trends in oceanic kinetic energy (Fig. 6c), whereas wind intensity increased mostly in the Southern Oceans (Dangendorf et al. 2019, discussed how this increase impacts sea level acceleration) while OKE increased everywhere except the subpolar regions (70° N and 70° S). As shown in Fig. 5, in subtropical regions there is increase in both, OKE and CUR, which suggests that Sverdrup-driven flows play some role. Ocean vorticity (Fig. 6d), which represents intensity and rotation direction of ocean eddies and gyres, shows less coherent trend pattern than OKE does. It is likely that each region is driven by local wind patterns and meso-scale eddies, so that latitudinal means may not represent significant trends. However, the statistically significant change in vorticity may indicate regional climatic changes in oceanic eddies, as some observations suggested (e.g., Beal and Elipot 2016; Martínez-Moreno et al. 2021).

3.2 Regional changes near western boundary currents (WBC)

Regional changes were analyzed in areas near 5 WBCs: 2 in the Northern Hemisphere (GS and KC) and 3 in the Southern Hemisphere (BC, AGC, and EAC). In these regions, WBCs as warm ocean currents, transport warmer subtropical waters poleward, thus creating areas with large SST gradients that resulted in large SSH gradients (Fig. 7) and strong geostrophic currents. Because of the close relation of SST and SSH, these WBCs can easily be detected from the RecSL data (Ezer and Dangendorf 2020). Moreover, the WBCs are not only regions of strong currents, but also regions of significant mesoscale variability and oceanic eddies that could contribute to OKE.

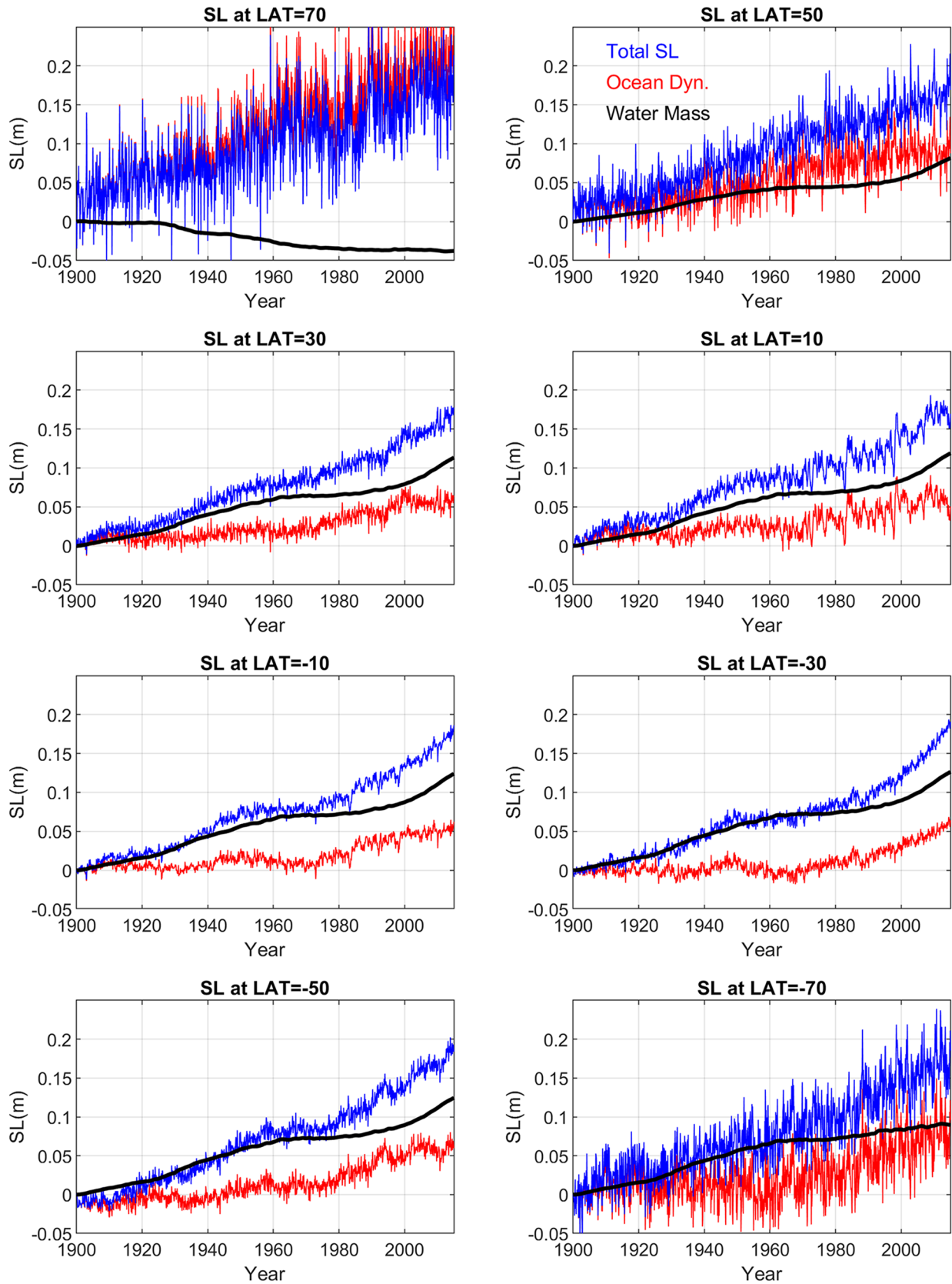


Fig. 3 Latitudinal averaged monthly sea level. Blue, red and black lines represent the total sea level, the SDSL contribution and the GRD contribution, respectively

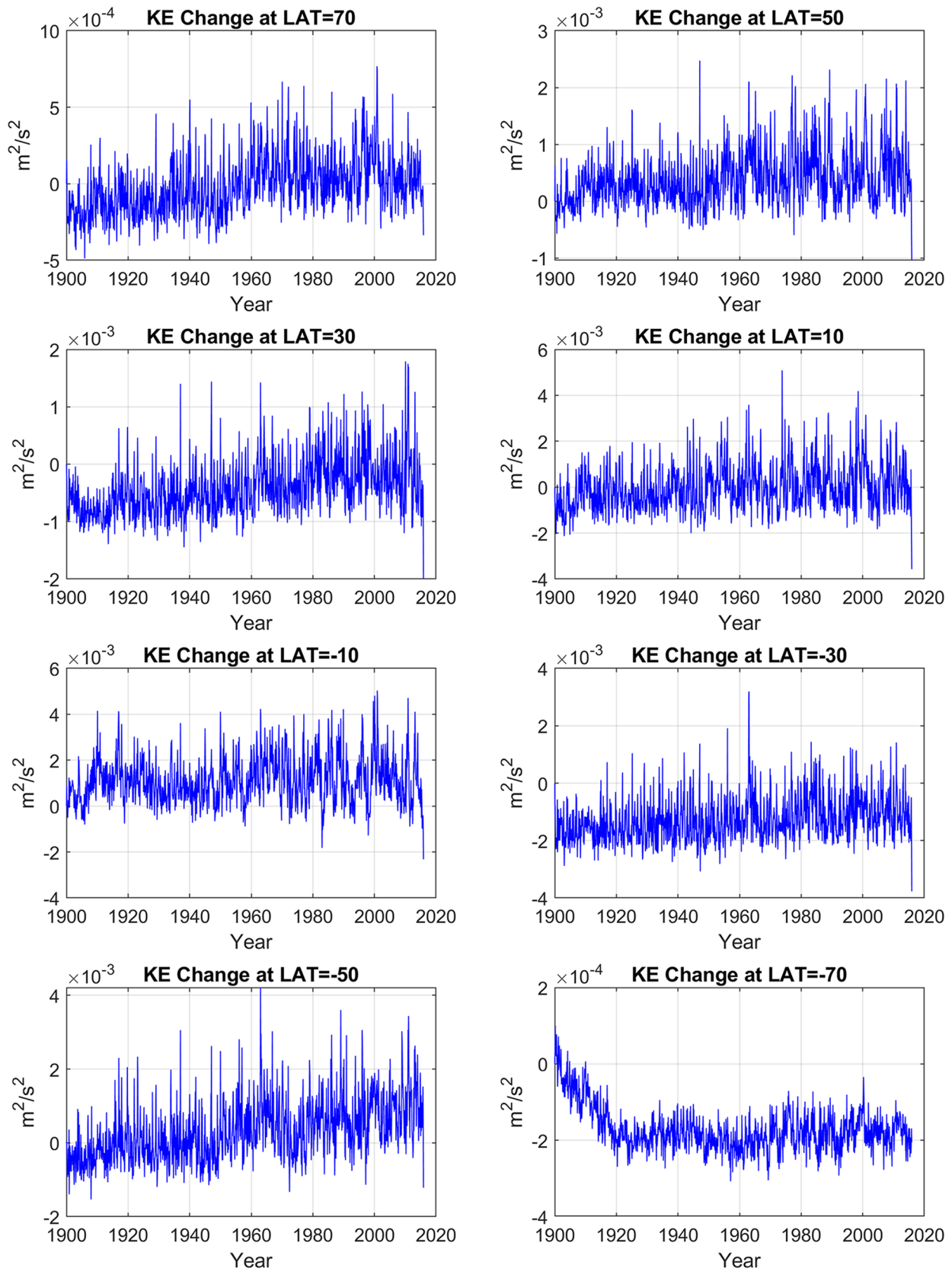


Fig. 4 Latitudinal averaged monthly mean oceanic kinetic energy (OKE) change (relative to 1900) calculated from sea level gradients and the geostrophic assumption (see text)

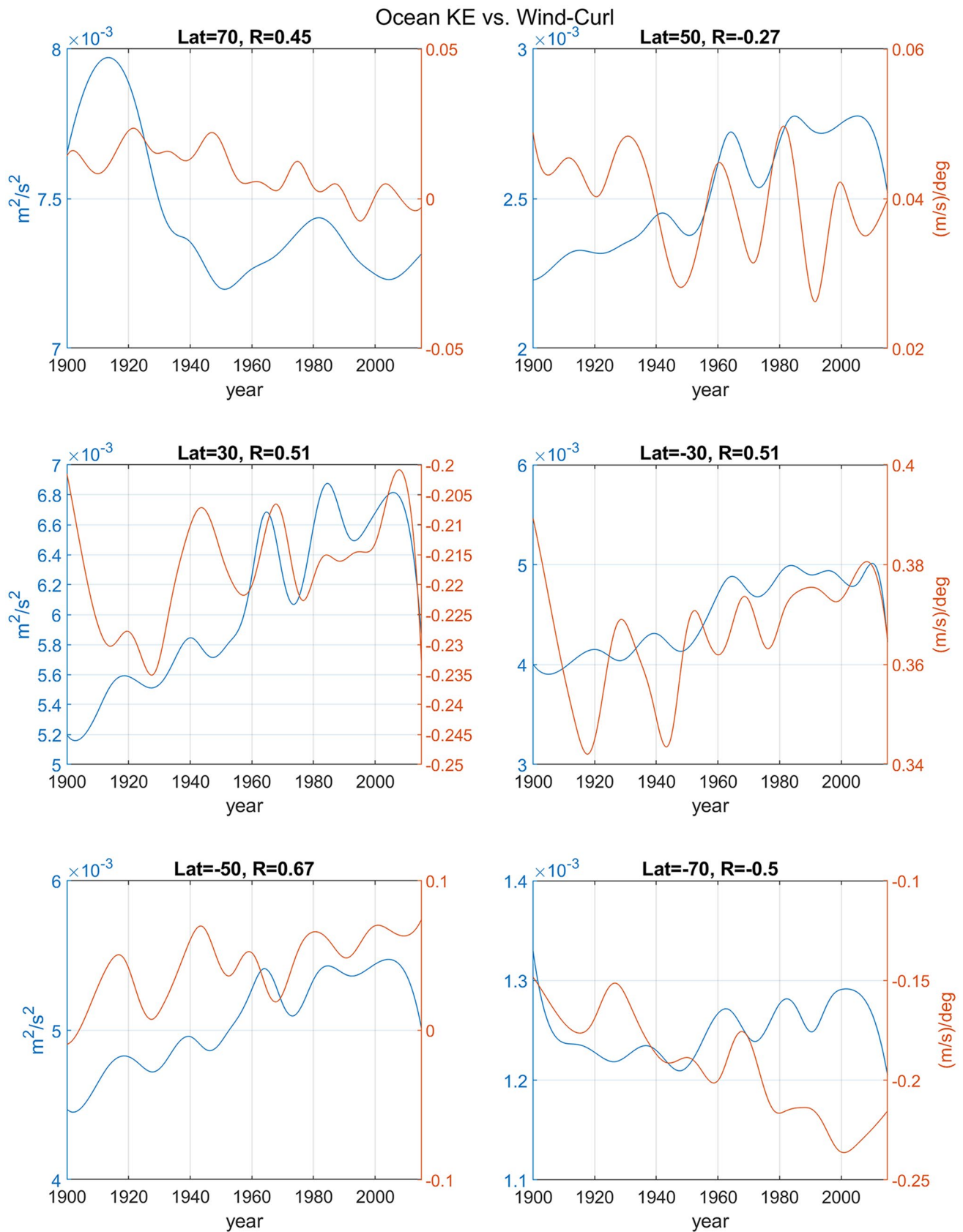


Fig. 5 Low frequency variations in OKE (blue lines; axis on the left) and variations in wind stress curl (CUR) (red lines; axis on the right). Correlation coefficient (R) for each latitude is indicated

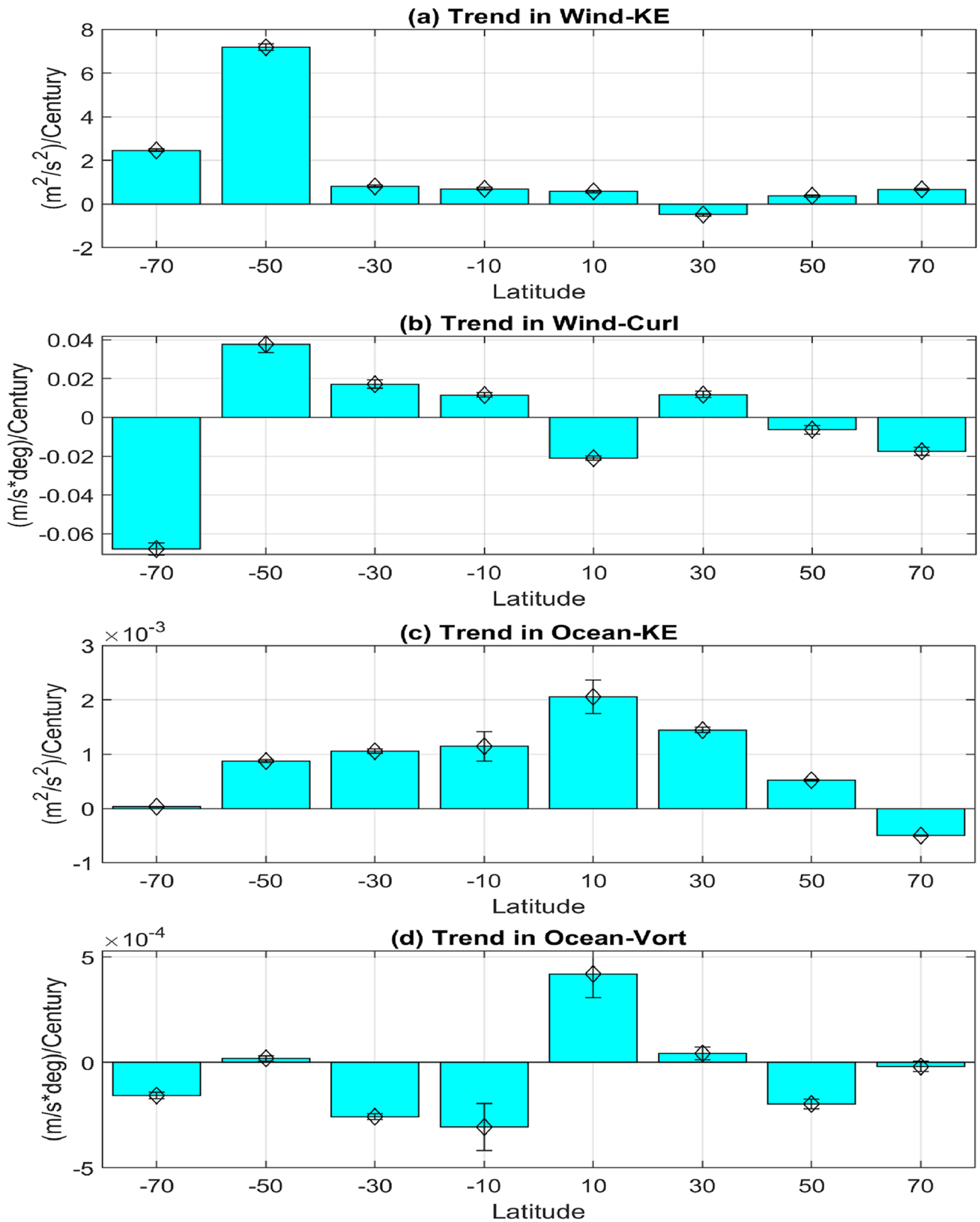


Fig. 6 Mean and error bars of trends in wind and oceanic properties for different latitudes: **a** wind kinetic energy (WKE), **b** wind stress curl (CUR), **c** oceanic kinetic energy (OKE), and **d** oceanic vorticity (VOR)

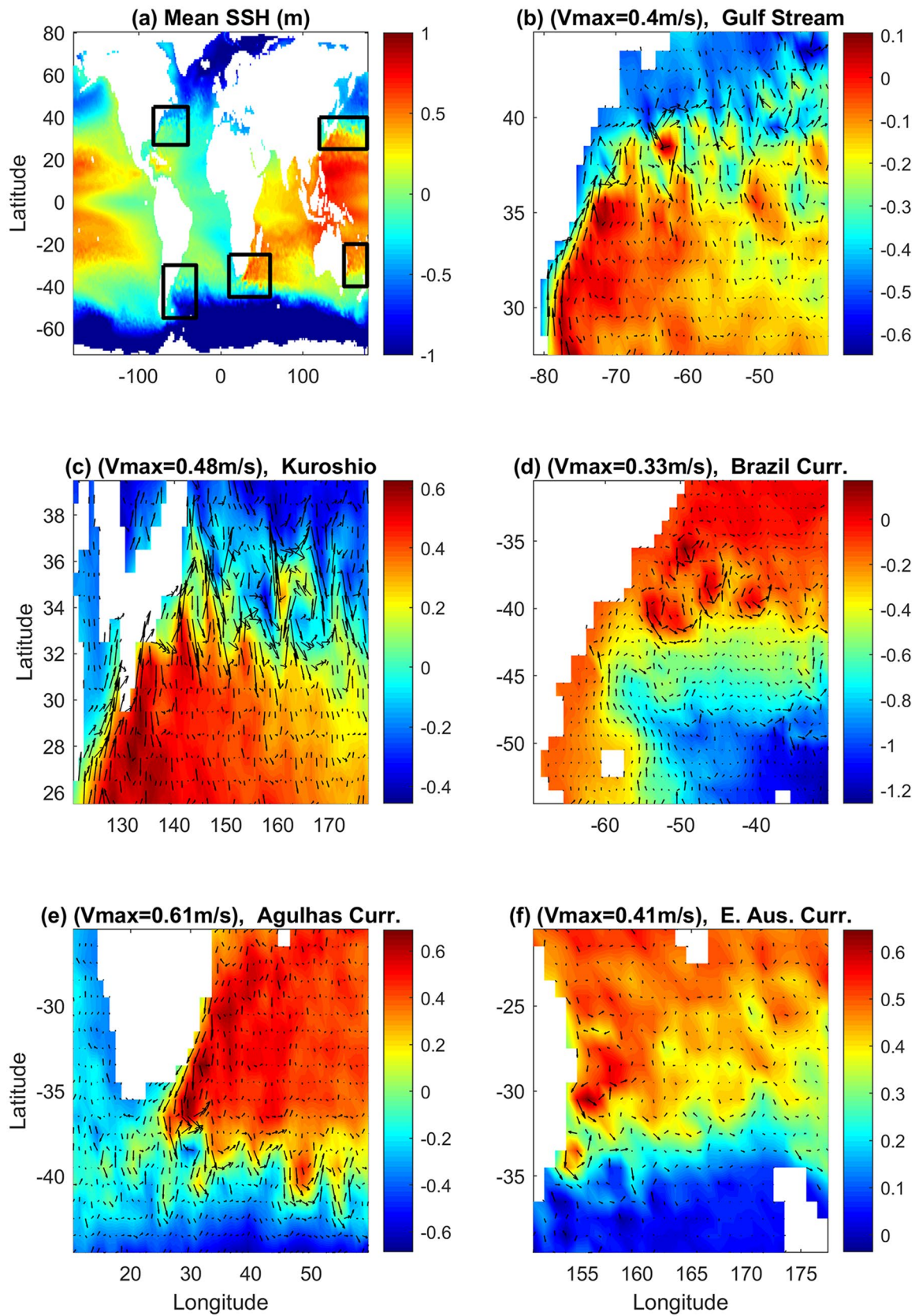


Fig. 7 **a** Global mean sea surface height (SSH) in RecSL and locations of 5 subregions near WBCs. **b–f** Mean SSH and surface velocity at: Gulf Stream (GS), Kuroshio Current (KC), Brazil Current (BC), Agulhas Current (AGC), and East Australian Current (EAC), respectively. The maximum geostrophic velocity obtained from the mean RecSL in each region is indicated

3.2.1 Regional sea level rise

Before looking at the century-long sea level record, it is constructive to evaluate the regional RecSL against altimeter data and against the global mean sea level (Fig. 8). Even though the altimeter data is not independent of RecSL and is used in the reconstruction to extract spatial modes (see Sect. 2) comparison between altimeter data and RecSL can tell us how well the RecSL can retain time-dependent variability and trends. The mean correlation in the 5 regions between the RecSL and the altimeter data is $R = 0.85 \pm 0.05$, which is consistent with previous results (Dangendorf et al. 2019; Ezer and Dangendorf 2020). Note however, that somewhat lower correlation ($R = 0.76$) is found near the GS where the RecSL data rely on more tide gauge data, but higher correlation ($R = 0.9$) is found in the EAC region where the RecSL data rely more on altimeter data due to lack of tide gauges there. The mean difference in the trend between the RecSL and the altimeter data is only ~ 0.4 mm/year. Both time series show considerable regional interannual variations (about ± 50 mm) relative to the global mean sea level, but these variations are distinctly different for each region. Therefore, both sea level variability and sea level rise trends are quite different for each WBC region, where trends during 1993–2015 vary between 2.4 mm/year in the GS region to 4.6 mm/year in the EAC region.

Since 1900, the regional sea level variability and SLR in the 5 WBCs regions can depart significantly from the global mean values and this is shown in Fig. 9. SLR is calculated over 3 different periods (I: 1900–1940, II: 1940–1980 and III: 1980–2015) to show the non-linear temporal changes. Global mean SLR and SLR in all regions show the slowest rates during period II and fastest rates during period III after 1980, in agreement with the multi-decadal global SLR pattern shown by Dangendorf et al. (2019). However, Dangendorf et al. (2019), Frederikse et al. (2020) and many other studies of global variations in sea level acceleration did not look at regional trends near WBCs. This result, of small deceleration in SLR from the 1920s to the 1960s and large acceleration from the 1960s to today, indicates that the barystatic sea level change (Fig. 2b) dominates all regions of the ocean. However, there are also considerable regional differences in SLR as seen by the acceleration rates. Between periods I and II, the global acceleration was negative and negligibly small (-0.0035 mm/year²) but the regional acceleration rates significantly change between regions

($+0.01$, -0.027 , -0.015 , -0.014 and $+0.0005$ mm/year², for GS, KC, BC, AGC and EAC, respectively). However, during recent time between periods II and III the global positive acceleration ($+0.033$ mm/year²) was (except one region) less than the regional acceleration ($+0.016$, $+0.039$, $+0.053$, $+0.054$ and $+0.076$ mm/year², for GS, KC, BC, AGC and EAC, respectively). The results are generally consistent with Dangendorf et al. (2019) who showed persistent global positive acceleration after the 1960s. There are other apparent regional differences, for example, in the southern hemisphere the BC and AGC which reside in a relatively close proximity, both show a long period since the 1940s with regional sea level higher than the global sea level, while the EAC shows regional sea level lower than the global from 1900 until the 1990s, with large acceleration after the 1990s. In the northern hemisphere the GS shows the largest interannual variability while the KC shows larger inter decadal variability.

3.2.2 Regional kinetic energy of the wind (WKE) and the ocean (OKE)

As previously shown (Figs. 4, 6), a significant increase in OKE is seen from 50°S to 50°N, while most of the increase in WKE is found south of 50°S, thus one may conclude that OKE and WKE may not be directly related, at least on a latitudinal averaged basis. However, subtropical gyres and WBCs are largely wind driven, so it is useful to evaluate this relation on a regional basis. Figure 10 compares the regional averaged WKE and OKE at the 5 WBCs areas. While both, OKE and WKE show considerable high-frequency and interannual variations, the low-frequency oscillations and the trends are very revealing. The upward trends in OKE at the 5 sites are surprisingly very similar, ranging from 18.8% increase per century at BC to 26.2% at KC and EAC. On the other hand, the trend of WKE over the same regions change widely from region to region with a decline of 10.9% per century in the GS region to an increase of 27.5% in the BC region. This regional discrepancy between WKE and OKE is consistent with the latitudinal results of Fig. 6. Decadal variabilities in the wind and the ocean are also very different, with coherent patterns across regions in the OKE (right panels of Fig. 10), but almost no coherency in the regional WKE (left panels of Fig. 10). A closer look at the low-frequency variability (Fig. 11) shows for example, a coherent minimum in OKE around 1945–1950 and maxima in almost all regions around 1965 and 1980. The correlation of low-frequency variability in OKE and WKE is statistically significant at 95% only for the KC region ($R = 0.49$), though in the BC and AGC regions positive correlations are significant at the 90% level. In the GS and EAC there is negative correlation (significant at 90% for EAC). Therefore, it seems that

Fig. 8 Area averaged sea level change in the 5 WBC regions (see locations in Fig. 7) during the altimeter era (1993–2015), comparing the global mean sea level (green), the altimeter data (red) and the RecSL (blue). Indicated in each panel are altimeter versus RecSL correlation (R) and sea level trends in the altimeter data (T_{alt}) and in the reconstruction data (T_{rec})

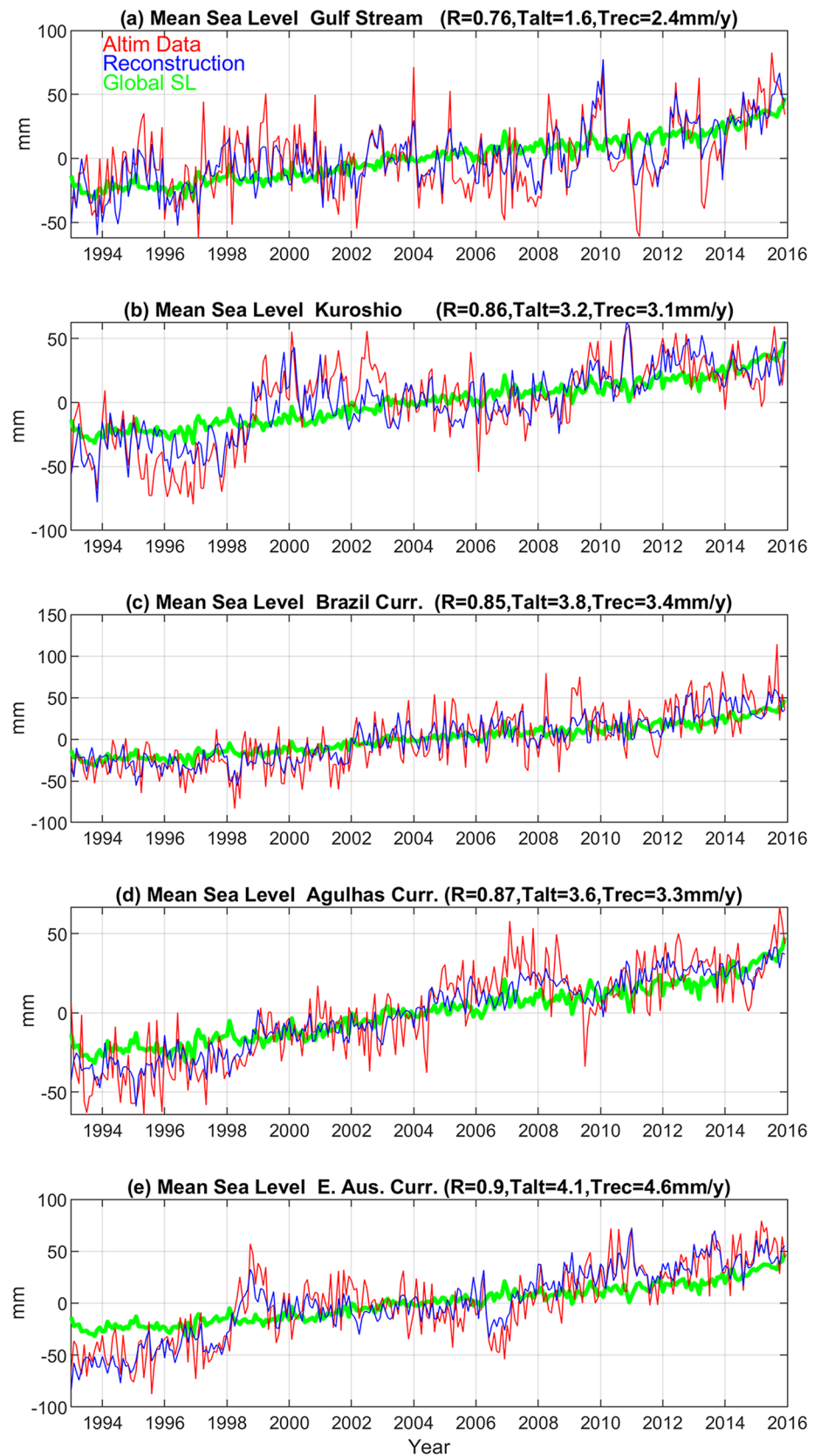
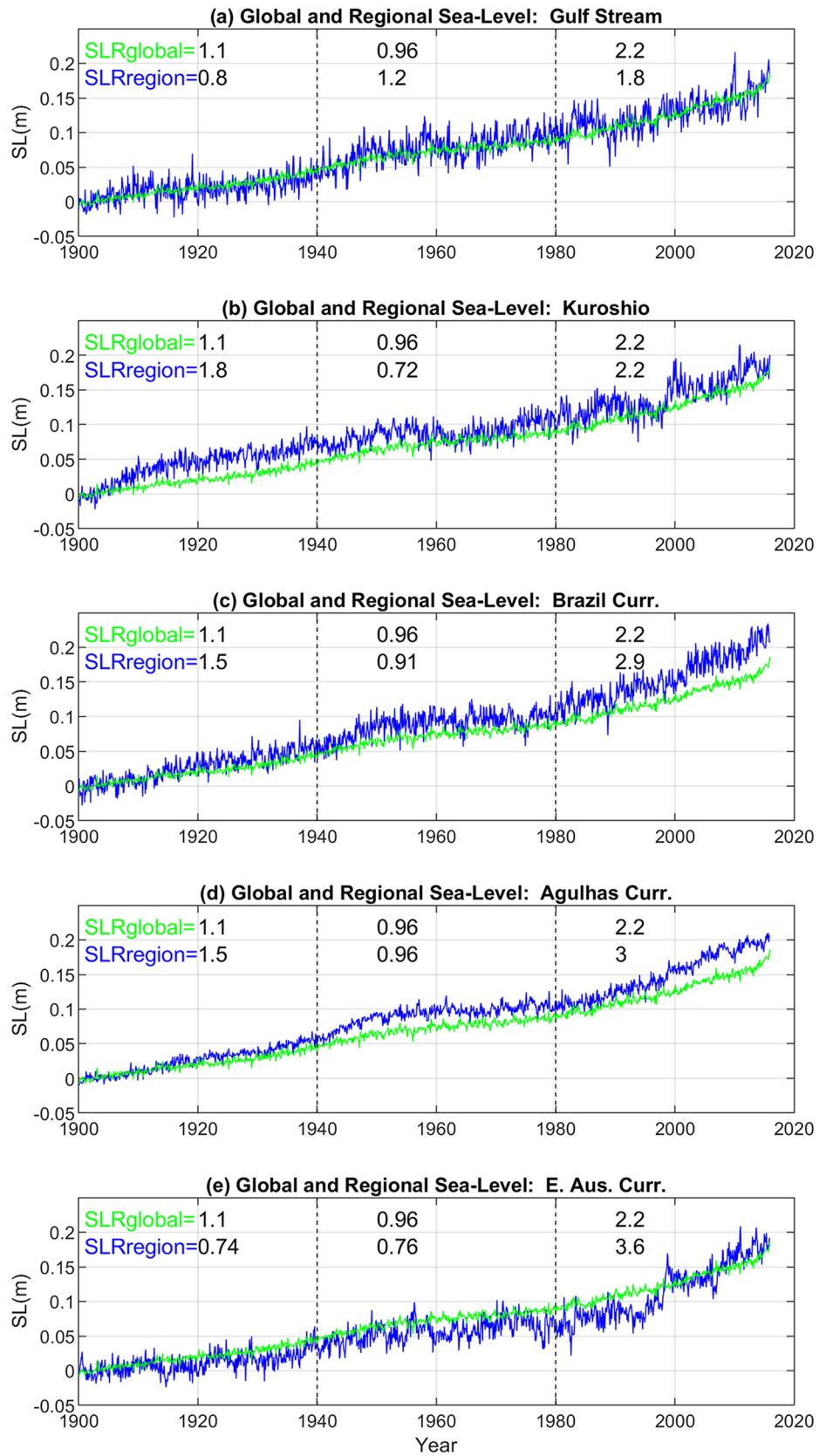


Fig. 9 Global mean sea level (green) and regional mean sea level (blue) at the 5 regions near WBCs. The global sea level rise (“SLRglobal”) and the regional sea level rise (“SLRregion”) rates (in mm/y) for 3 periods are indicated: 1900–1940, 1940–1980, and 1980–2015



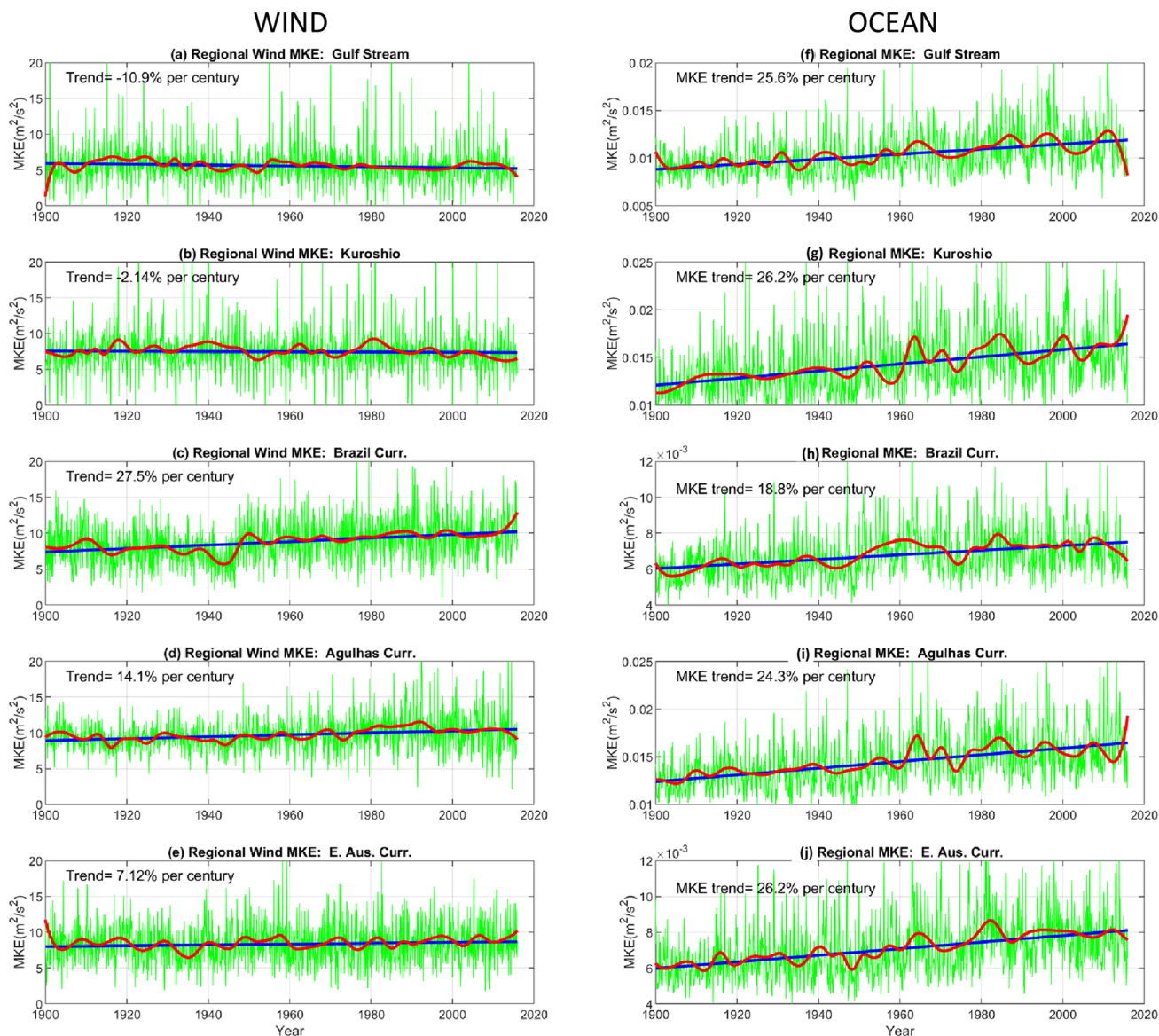


Fig. 10 Regional wind kinetic energy (WKE; left panels) and ocean kinetic energy (OKE; right panels) for the 5 regions shown in Fig. 7. Green lines are monthly data, red lines are low frequency variations

and blue lines are the linear trends (with values indicated in each panel). The low-passed filtered variations were obtained from the sum of low frequency EMD modes and the EMD residual trend (see text)

long-term changes in wind intensity contribute to OKE in some regions more than others, pointing to regional dynamics with different forcing at each region. The high correlation between OKE and WKE near the Kuroshio and the decadal pattern in Fig. 11b are consistent with studies that show a wind-driven intensification of the KC from the 1970s to the 1980s (Deser et al. 1999).

So far, only area averaged values of OKE and WKE were evaluated, but this approach neglects the local pattern of the wind and the ocean dynamics, so that now local correlations are considered in Fig. 12. The local OKE-WKE correlation patterns (left panels of Fig. 12) show that in each region there are areas with significant positive correlations (red

colors with no contours), but also areas with negative (blue) or insignificant (contoured) correlations (95% significant level is obtained for absolute value of R larger than about 0.08). It seems that area-averaged calculations, as done before, may not capture the full picture of the wind-ocean relation. Note also that even in regions with statistically significant correlation (maximum correlation $R \sim 0.3$), the wind is responsible for only $\sim 10\%$ of the total variability, since mesoscale eddies and meandering of WBCs dominate the variability. In the EAC region, for example (Fig. 12i), positive OKE-WKE correlation is found over the warm subtropical south Pacific region (Fig. 7f) while negative correlations are found in the colder southern region near the Antarctic

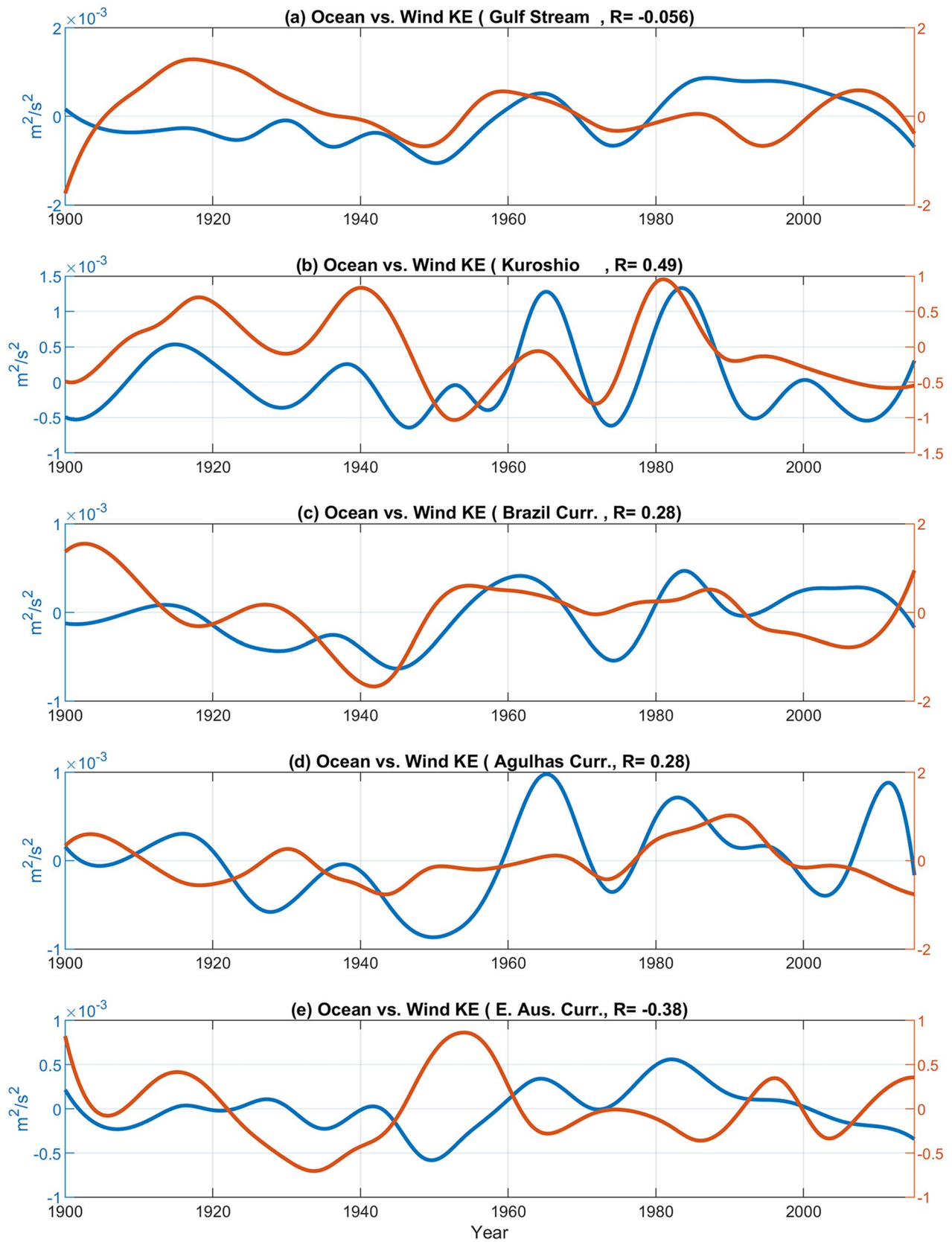


Fig. 11 Low-passed filtered variations (sum of the low frequency oscillating EMD modes in Fig. 10, but without the EMD residual trend) of OKE (blue; axis on left) and WKE (red; axis on right) in the 5 regions shown in Fig. 7. Correlation coefficient (R) is shown for each region

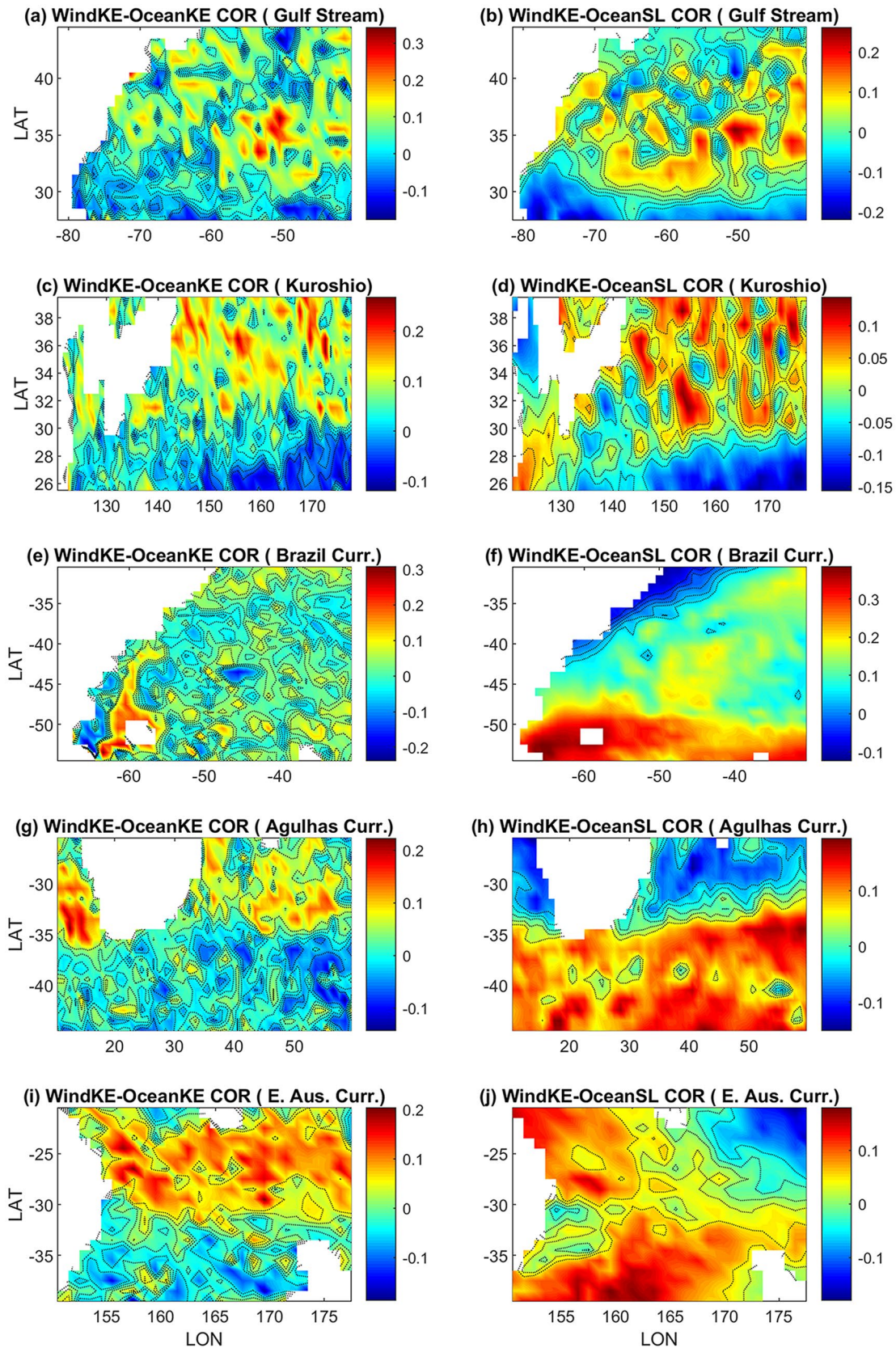


Fig. 12 Correlation coefficient between WKE and OKE (left panels) and between WKE and ocean sea level anomaly (right panels) for the 5 WBCs regions. Red and blue colored areas cleared of contours indicate regions with confidence level above 95% for positive and negative correlations, respectively

Circumpolar Current (ACC), and similar pattern is seen in the AGC region (Figs. 7e, 12g). The right panels of Fig. 12 show the correlation of WKE with sea level anomaly, demonstrating that the wind is significantly correlated with sea level over large portions of each domain, especially in the southern hemisphere (Fig. 12f, h, j). For example, significant WKE-sea level correlations are seen in all the BC area except the coast (i.e., Fig. 12f is almost clear of contours, so the entire region is significantly wind-driven). In the WBCs of the northern hemisphere (GS and KC in Fig. 12b, d) the WKE-sea level correlation is noisy and less clear in its pattern, since these regions are dominated by meso-scale eddies which are not driven by wind. The results demonstrate the complex interconnections between SST, SSH, WKE and OKE, so separating between the forcing is not possible due to feedbacks between the different factors. If SST is the driven force, spatially uneven warming would affect sea level through the steric relation but would also affect wind patterns. However, if wind and water mass changes drive sea level variability, the dynamics of WBCs (and thus OKE) would change as well, which could cause changes in SST through advective processes.

As seen in Fig. 2, SLR due to changes in GRD and SDSL had increased significantly, especially after the 1980s, so it is constructive to evaluate if those changes are reflected in the pattern of the wind and the ocean currents. Figure 13 compares the recent changes (1980–2015 versus 1940–1980) in wind speed and direction (left panels), in ocean currents (middle panels), and in sea level (right panels). These two periods represent a time of relatively slow SLR versus a time of fast SLR (Fig. 9). It is quite clear that variations in the wind patterns are generally different in each region, though in general, in most regions one can see an increased cyclonic wind pattern, thus an increased wind stress curl (as seen in Fig. 5) which will support stronger flows in subtropical gyres. However, local changes vary from region to region. In the GS region for example, stronger southwestward wind along the coast (Fig. 13a) would oppose the GS flow in the South Atlantic Bight, but increase recirculation in the Mid-Atlantic Bight, as reflected in the change in ocean currents (Fig. 13b); this may explain the poor OKE-WKE correlation there (Figs. 11a, 12a). Similar wind pattern change is seen in the EAC region (Fig. 13m) where OKE–WKE correlations are also negative (Fig. 11e). The changes in sea level (right panels of Fig. 13) are very consistent with the changes in ocean currents (middle panels in Fig. 13), showing that the areas with the largest spatial variations in sea level are

those with the largest changes in ocean currents. The spatial changes in sea level seen here are due to the SDSL change (see Figs. 1f, 2c) and they are consistent with steric sea level changes (e.g., see Extended Fig. 4 in Frederikse et al. 2020). In the BC and EAC regions where the increased sea level is more even (Fig. 13i, o) the change in WBCs is relatively small, while in the other regions large spatial variations in sea level resulted in large local changes near strong oceanic currents. In the AGC region, changes are mostly along the ACC while there is almost no change in the Agulhas Current itself along the African coast, which is consistent with observations that show broadening, but not strengthening in the Agulhas Current since the early 1990s (Beal and Elipot 2016). The changes in sea level seen here are also consistent with previous studies that showed enhanced warming near subtropical WBCs (Wu et al. 2012; Yang et al. 2016), but here we show that the warming is uneven and thus leading to increase sea level gradients and kinetic energy.

4 Summary and conclusions

A recent study (Ezer and Dangendorf 2020) demonstrated the ability of the reconstructed sea level of Dangendorf et al. (2019) to detect century-long (1900–2015) dynamic changes in one WBC, the Gulf Stream. As a follow up, the main goal here was to expand this approach and to explore global and regional long-term changes in ocean currents through analysis of oceanic kinetic energy derived from the same reconstructed sea level. Several studies suggested that WBCs are intensifying under warming climate conditions (Deser et al. 1999; Ridgway 2007; Goni et al. 2011; Wu et al. 2012; Yang et al. 2016). These studies suggested that the primary reason for the WBCs intensification is a shift and increased strength of the wind, especially in the southern hemisphere (Cai 2006; Hu et al. 2020), though some studies suggested that warming of sea surface temperatures contributes more than changes in the wind to the intensification of some WBCs (Chen et al. 2019). One aspect that has not been addressed in those studies was the impact on ocean dynamics from water mass changes such as the land-based ice melting near Greenland and Antarctica. Changes in water masses play a major role in the sea level rise budget, as shown recently by Frederikse et al. (2020). Therefore, in our study, in addition to considering the role of the wind, we separated SLR into two components: barystatic-driven (GRD) sea level and dynamic-driven (SDSL) sea level. The dynamic sea level change includes all the elements besides barystatic sea level, i.e., changes in wind, steric temperature and salinity, and ocean circulation. Climate change results in increased global mean ocean temperatures, global wind speed and global ocean kinetic energy (Hu et al. 2020;

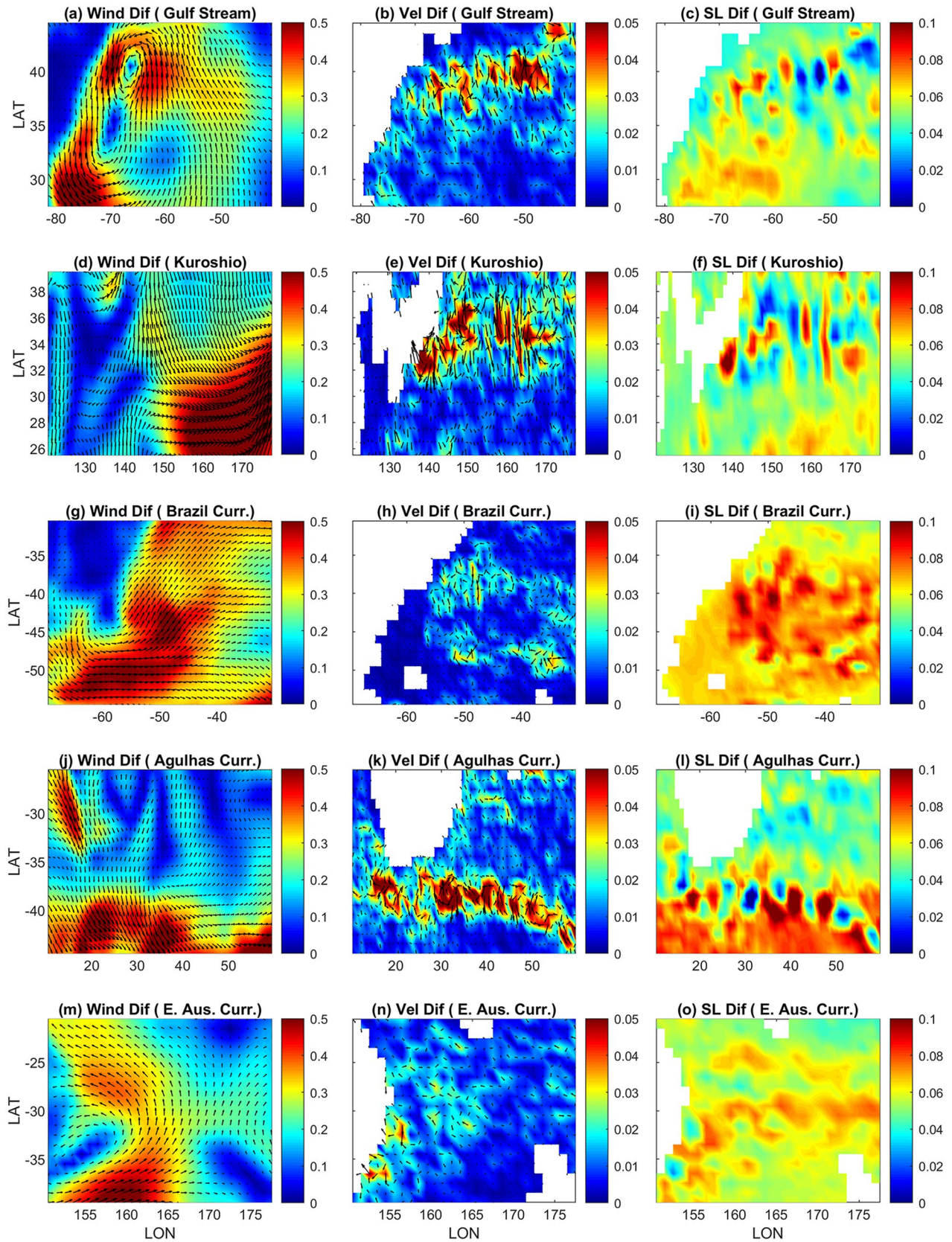


Fig. 13 Changes between 1940–1980 and 1980–2015 (the last 2 periods in Fig. 9) for the 5 WBC regions (each row for different region). Left panels: change in wind speed (m/s) in color (red- largest change) and direction (arrows). Middle panels: change in ocean currents (m/s). Right panels: change in sea level (m)

Martínez-Moreno et al. 2021), but there are also large differences between the response of individual WBCs to global warming (Sen Gupta et al. 2021), for example, the projection of Gulf Stream weakening, but Kuroshio Current strengthening (Chen et al. 2019). Therefore, we wanted to investigate regional changes in each WBC.

The analysis showed very different spatial and temporal variability in the barostatic and dynamic sea level. GRD is linked to a coherent spatial sea level rise away from polar regions and large sea level drop near ice melting high latitude regions- these changes in meridional gradients of sea level can contribute to increased OKE. Temporal variations associated with GRD include very long time-scale changes with an apparent ~60 to 80 years cycle that resembles the global 60-year sea level cycle discussed by Chambers et al. (2012). However, the GRD pattern seen here (Fig. 2b) and discussed in Frederikse et al. (2020) indicates that this may not be a natural cycle linked to AMO, as suggested by Chambers et al. (2012) and others, but rather a water mass change that slowed down SLR in the 1970s due to anthropogenic massive water impoundment by dams in the 1970s (Chao et al. 2008), which followed by accelerated SLR due to increased ice loss in the 1990s and 2000s. The impact of SDSL is very different than that of GRD, it is responsible for producing small-scale spatial variability and shorter-term temporal variability in sea level and OKE. The SDSL in middle latitudes dominate recent variability and contributed to acceleration in SLR after the 1960s, as indicated here (Figs. 3, 9) and in Dangendorf et al. (2019). On latitudinal averaged basis, increased wind speed and thus WKE does not seem to be the main cause for the increase in OKE- most of the increased WKE found in the Southern Ocean south of 50° S, while OKE almost evenly increased in middle latitudes 50° S–50° N. However, over subtropical regions (e.g., at 30° S and 30° N) increased wind stress curl (CUR) is correlated with increased OKE, pointing to potential contribution from Sverdrup transports.

Analysis of changes near WBCs reveals some similarity and some regional differences. Consistent with the long-term global signal of the GRD, area mean SLR in all 5 regions had the slowest SLR rate during 1940–1980, the fastest rate after 1980 and a moderate rate before 1940. However, due to SDSL, there are differences in the interannual variations of sea level between the WBCs. As seen in the latitudinal averaged results, there is no clear correlation between WKE and OKE that apply to all regions—the upward trend in OKE is very similar for all regions, while WKE trends vary wildly

(negative in the WBCs of the northern hemisphere and positive in WBCs of the southern hemisphere). Decadal variations in WBCs are also similar for OKE but very different for WKE, so for example OKE-WKE correlation is $R = +0.49$ in the KC region, but $R = -0.38$ in the EAC region. In fact, WKE in many regions is better correlated with SSH (probably due to the tight SST-SSH connection) than with OKE. Therefore, we can conclude that on the time and space scales that the RecSL provides, intensification of wind speed is not the main driver of local changes to ocean currents (high frequency and seasonal wind variability can induce local ocean currents, but they are not considered here). So, what are the mechanisms involved in the increase of OKE near WBCs? Close examination of the regional changes in wind and sea level patterns near WBCs during the period of increased SLR shows a combination of more cyclonic wind circulation (wind stress curl effect) and increased warming near WBCs (Yang et al. 2016; Chen et al. 2019) that created large spatial variations in SSH (resembling the steric sea level changes; Frederikse et al. 2020). Larger spatial variations increased OKE through geostrophic currents and eddies (Martínez-Moreno et al. 2021; Beal and Elipot (2016) for example, observed an increase in eddy activities near the Agulhas Current. One should note however that each region has its own unique characteristics and different response to climate change, as summarized in Fig. 13. The study demonstrates the usefulness of global reconstructions for studies of regional ocean dynamics, but it also shows the complexity of regional dynamics, especially near western boundary currents. To get a better understanding of the mechanisms involved, it would be useful to follow this study with sensitivity numerical simulations that could potentially separate the different processes highlighted here.

Acknowledgements The study is part of Old Dominion University's Climate Change and Sea Level Rise Initiative at the Institute for Coastal Adaptation and Resilience (ICAR). The Center for Coastal Physical Oceanography (CCPO) provided facility and computational resources. The altimeter data is available from the Copernicus Marine service (<https://marine.copernicus.eu/>) and the RecSL data is available by request from the authors.

References

- Andres M, Donohue KA, Toole JM (2020) The Gulf Stream's path and time-averaged velocity structure and transport at 68.5° W and 70.3° W. *Deep Sea Res Part I*. <https://doi.org/10.1016/j.dsr.2019.103179>
- Baringer MO, Larsen JC (2001) Sixteen years of florida current transport at 27° N. *Geophys Res Lett* 28(16):3179–3182. <https://doi.org/10.1029/2001GL013246>
- Beal LM, Elipot S (2016) Broadening not strengthening of the Agulhas current since the early 1990s. *Nature*. <https://doi.org/10.1038/nature19853>

- Blaha JP (1984) Fluctuations of monthly sea level as related to the intensity of the Gulf Stream from Key West to Norfolk. *J Geophys Res* 89(C5):8033–8042. <https://doi.org/10.1029/JC089iC05p08033>
- Blaker ET, Hirschi JM, McCarthy G, Sinha B, Taws S, Marsh R, Coward A, de Cuevas B (2014) Historical analogues of the recent extreme minima observed in the Atlantic meridional overturning circulation at 26° N. *Clim Dyn* 44(1–2):457–473. <https://doi.org/10.1007/s00382-014-2274-6>
- Bryden HL, Longworth HR, Cunningham SA (2005) Slowing of the Atlantic meridional overturning circulation at 25° N. *Nature* 438:655–657. <https://doi.org/10.1038/nature04385>
- Caesar L, Rahmstorf S, Robinson A, Feulner G, Saba V (2018) Observed fingerprint of a weakening Atlantic Ocean overturning circulation. *Nature* 556:191–196. <https://doi.org/10.1038/s41586-018-0006-5>
- Cai W (2006) Antarctic ozone depletion causes an intensification of the Southern Ocean super-gyre circulation. *Geophys Res Lett* 33:L03712. <https://doi.org/10.1029/2005GL024911>
- Calafat FM, Chambers DP, Tsimplis MN (2014) On the ability of global sea level reconstructions to determine trends and variability. *J Geophys Res* 119:1572–1592. <https://doi.org/10.1002/2013JC009298>
- Chambers DP, Merrifield MA, Nerem RS (2012) Is there a 60-year oscillation in global mean sea level? *Geophys Res Lett* 39:L18607. <https://doi.org/10.1029/2012GL052885>
- Chao BF, Wu YH, Li YS (2008) Impact of artificial reservoir water impoundment on global sea level. *Science* 11(320):212–214. <https://doi.org/10.1126/science.1154580>
- Chen C, Wang G, Xie S, Liu W (2019) Why does global warming weaken the Gulf Stream but intensify the Kuroshio? *J Clim* 32:7437–7451. <https://doi.org/10.1175/JCLI-D-18-0895.1>
- Church JA, White NJ (2006) A 20th century acceleration in global sea-level rise. *Geophys Res Lett*. <https://doi.org/10.1029/2005GL024826>
- Church JA, White NJ (2011) Sea-level rise from the late 19th to the early 21st century. *Surv Geophys* 32:585–602. <https://doi.org/10.1007/s10712-011-9119-1>
- Church JA, White NJ, Konikow LF, Domingues CM, Cogley JG, Rignot E, Gregory JM, van den Broeke MR, Monaghan AJ, Velicogna I (2011) Revisiting the Earth's sea-level and energy budgets from 1961 to 2008. *Geophys Res Lett* 38:L18601. <https://doi.org/10.1029/2011GL048794>
- Compo GP, Whitaker JS, Sardeshmukh PD, Matsui N, Allan RJ, Yin X, Gleason BE, Vose RS, Rutledge G, Bessemoulin P, Brönnimann S, Brunet M, Crouthamel RI, Grant AN, Groisman PY, Jones PD, Kruk MC, Kruger AC, Marshall GJ, Maugeri M, Mok HY, Nordli Ø, Ross TF, Trigo RM, Wang XL, Woodruff SD, Worley SJ (2011) The twentieth century reanalysis project. *Q J R Meteorol Soc* 137:1–28. <https://doi.org/10.1002/qj.776>
- Dangendorf S, Rybski D, Mudersbach C, Müller A, Kaufmann E, Zorita E, Jensen J (2014) Evidence for long-term memory in sea level. *Geophys Res Lett* 41:5564–5571. <https://doi.org/10.1002/2014GL060538>
- Dangendorf S, Marcos M, Wöppelmann G, Conrad CP, Frederikse T, Riva R (2017) Reassessment of 20th century global mean sea level rise. *Proc Natl Acad Sci* 114(23):5946–5951. <https://doi.org/10.1073/pnas.1616007114>
- Dangendorf S, Hay C, Calafat FM, Marcos M, Piecuch CG, Berk K, Jensen J (2019) Persistent acceleration in global sea-level rise since the 1960s. *Nat Clim Change* 9:705–710. <https://doi.org/10.1038/s41558-019-0531-8>
- Deser C, Alexander M, Timlin M (1999) Evidence for a wind-driven intensification of the Kuroshio current extension from the 1970s to the 1980s. *J Clim* 12(6):1697–1706. [https://doi.org/10.1175/1520-0442\(1999\)012%3c1697:EFWDI%3e2.0.CO;2](https://doi.org/10.1175/1520-0442(1999)012%3c1697:EFWDI%3e2.0.CO;2)
- Dong S, Baringer MO, Goni GJ (2019) Slow down of the Gulf Stream during 1993–2016. *Sci Rep* 9:6672. <https://doi.org/10.1038/s41598-019-42820-8>
- Enfield DB, Mestas-Nunez AM, Trimble PJ (2001) The Atlantic Multidecadal oscillation and its relationship to rainfall and river flows in the continental U.S. *Geophys Res Lett* 28(10):2077–2080. <https://doi.org/10.1029/2000GL012745>
- Ezer T (1999) Decadal variabilities of the upper layers of the subtropical North Atlantic: an ocean model study. *J Phys Oceanogr* 29(12):3111–3124. [https://doi.org/10.1175/1520-0485\(1999\)029](https://doi.org/10.1175/1520-0485(1999)029)
- Ezer T (2001) Can long-term variability in the Gulf Stream transport be inferred from sea level? *Geophys Res Lett* 28(6):1031–1034. <https://doi.org/10.1029/2000GL011640>
- Ezer T (2015) Detecting changes in the transport of the Gulf Stream and the Atlantic overturning circulation from coastal sea level data: the extreme decline in 2009–2010 and estimated variations for 1935–2012. *Glob Planet Change* 129:23–36. <https://doi.org/10.1016/j.gloplacha.2015.03.002>
- Ezer T, Dangendorf S (2020) Global sea level reconstruction for 1900–2015 reveals regional variability in ocean dynamics and an unprecedented long weakening in the Gulf Stream flow since the 1990s. *Ocean Sci* 16(4):997–1016. <https://doi.org/10.5194/os-2020-22>
- Ezer T, Atkinson LP, Corlett WB, Blanco JL (2013) Gulf Stream's induced sea level rise and variability along the U.S. mid-Atlantic coast. *J Geophys Res* 118:685–697. <https://doi.org/10.1002/jgrc.20091>
- Frederikse T, Landerer F, Caron L, Adhikari S, Parkes D, Humphrey VW, Dangendorf S, Hogarth P, Zanna L, Cheng L, Wu Y-H (2020) The causes of sea-level rise since 1900. *Nature* 584:393–397. <https://doi.org/10.1038/s41586-020-2591-3>
- Gehrels WR, Dangendorf S, Barlow NLM, Saher MH, Long AJ, Woodworth PL, Piecuch CG, Berk K (2020) A preindustrial sea-level rise hotspot along the Atlantic coast of North America. *Geophys Res Lett*. <https://doi.org/10.1029/2019GL085814>
- Goni GJ, Bringas F, DiNezio PN (2011) Observed low frequency variability of the Brazil current front. *J Geophys Res* 116:C10037. <https://doi.org/10.1029/2011JC007198>
- Greatbatch RJ, Fanning AF, Goulding AD, Levitus S (1991) A diagnosis of interpentadal circulation changes in the North Atlantic. *J Geophys Res* 96(C12):22009–22023. <https://doi.org/10.1029/91JC02423>
- Gregory JM, Griffies SM, Hughes CW, Lowe JA, Church JA, Fukimori I, Gomez N, Kopp RE, Landerer F, Le Cozannet G, Ponte RM, Stammer D, Tamisiea ME, van de Wal RSW (2019) Concepts and terminology for sea level: mean, variability and change, both local and global. *Surv Geophys* 40:1251–1289. <https://doi.org/10.1007/s10712-019-09525-z>
- Hamlington BD, Leben RR, Strassburg MW, Kim KY (2014) Cyclostationary empirical orthogonal function sea-level reconstruction. *Geosci Data J* 1:13–19. <https://doi.org/10.1002/gdj3.6>
- Han W, Stammer D, Thompson P, Ezer T, Palanisamy H, Zhang X, Domingues C, Zhang L, Yuan D (2019) Impact of basin-scale climate modes on coastal sea level: a review. *Surv Geophys* 40(6):1493–1541. <https://doi.org/10.1007/s10712-019-09562-8>
- Hay CH, Morrow E, Kopp RE, Mitrovica JX (2015) On the robustness of Bayesian fingerprinting estimates of global sea level change. *J Clim* 30:3025–3038. <https://doi.org/10.1175/JCLI-D-16-0271.1>
- Hu S, Sprintall J, Guan C, McPhaden MJ, Wang F, Hu D, Cai W (2020) Deep-reaching acceleration of global mean ocean circulation over the past two decades. *Sci Adv*. <https://doi.org/10.1126/sciadv.aax7727>
- Huang NE, Shen Z, Long SR, Wu MC, Shih EH, Zheng Q, Tung CC, Liu HH (1998) The empirical mode decomposition and the Hilbert

- spectrum for non stationary time series analysis. *Proc R Soc Lond Ser A* 45:903–995. <https://doi.org/10.1098/rspa.1998.0193>
- Jevrejeva S, Moore JC, Grinsted A, Woodworth PL (2008) Recent global sea level acceleration started over 200 years ago? *Geophys Res Lett* 35:L08715. <https://doi.org/10.1029/2008GL033611>
- Little CM, Hu A, Hughes CW, McCarthy GD, Piecuch CG, Ponte RM, Thomas MD (2019) The relationship between U.S. east coast sea level and the Atlantic meridional overturning circulation: a review. *J Geophys Res* 124:6435–6458. <https://doi.org/10.1029/2019JC015152>
- Lutjeharms JRE (2006) *The Agulhas current*. Springer
- Martínez-Moreno J, Hogg AM, England MH, Constantinou NC, Kiss AE, Morrison AK (2021) Global changes in oceanic mesoscale currents over the satellite altimetry record. *Nat Clim Change* 11:397–403. <https://doi.org/10.1038/s41558-021-01006-9>
- McCarthy G, Frejka-Williams E, Johns WE, Baringer MO, Meinen CS, Bryden HL, Rayner D, Duchez A, Roberts C, Cunningham SA (2012) Observed interannual variability of the Atlantic meridional overturning circulation at 26.5°N. *Geophys Res Lett*. <https://doi.org/10.1029/2012GL052933>
- Meinen CS, Baringer MO, Garcia RF (2010) Florida Current transport variability: an analysis of annual and longer-period signals. *Deep-Sea Res* 57(7):835–846. <https://doi.org/10.1016/j.dsr.2010.04.001>
- Merrifield MA, Merrifield ST, Mitchum GT (2009) An anomalous recent acceleration of global sea level rise. *J Clim* 22:5772–5781. <https://doi.org/10.1175/2009JCLI2985.1>
- Mizuno K, White WB (1983) Annual and interannual variability in the Kuroshio current system. *J Phys Oceanogr* 13:1847–1867. [https://doi.org/10.1175/1520-0485\(1983\)013<1847:AAVIT>2.0.CO;2](https://doi.org/10.1175/1520-0485(1983)013<1847:AAVIT>2.0.CO;2)
- Montgomery R (1938) Fluctuations in monthly sea level on eastern U.S. coast as related to dynamics of western North Atlantic Ocean. *J Mar Res* 1:165–185
- Piecuch CG (2020) Likely weakening of the Florida current during the past century revealed by sea-level observations. *Nat Commun*. <https://doi.org/10.1038/s41467-020-17761-w>
- Piecuch CG, Calafat FM, Dangendorf S, Jorda G (2019) The ability of Barotropic models to simulate historical mean sea level changes from coastal tide gauge data. *Surv Geophys* 40:1399–1435. <https://doi.org/10.1007/s10712-019-09537-9>
- Rahmstorf S, Box J, Feulner G, Mann ME, Robinson A, Rutherford S, Schaffernicht EJ (2015) Exceptional twentieth-century slowdown in Atlantic Ocean overturning circulation. *Nat Clim Chan* 5:475–480. <https://doi.org/10.1038/nclimate2554>
- Ridgway KR (2007) Long-term trend and decadal variability of the southward penetration of the East Australian Current. *Geophys Res Lett* 34:L13613. <https://doi.org/10.1029/2007GL030393>
- Roberts CD, Jackson L, McNeill D (2014) Is the 2004–2012 reduction of the Atlantic meridional overturning circulation significant? *Geophys Res Lett* 41:3204–3210. <https://doi.org/10.1002/2014GL059473>
- Rossby T, Flagg CN, Donohue K, Sanchez-Franks A, Lillibridge J (2014) On the long-term stability of Gulf Stream transport based on 20 years of direct measurements. *Geophys Res Lett* 41:114–120. <https://doi.org/10.1002/2013GL058636>
- Sallenger AH, Doran KS, Howd P (2012) Hotspot of accelerated sea-level rise on the Atlantic coast of North America. *Nat Clim Chan* 2:884–888. <https://doi.org/10.1038/NCILMATE1597>
- Sen Gupta A, Stellema A, Pontes GM, Taschetto AS, Verges A, Rossi V (2021) Future changes to the upper ocean Western Boundary Currents across two generations of climate models. *Sci Rep* 11:9538. <https://doi.org/10.1038/s41598-021-88934-w>
- Slangen A, Church J, Agosta C, Fettweis X, Marzeion B, Richter K (2016) Anthropogenic forcing dominates global mean sea-level rise since 1970. *Nat Clim Change* 6:701–705. <https://doi.org/10.1038/nclimate2991>
- Smeed DA, Josey SA, Beaulieu C, Johns WE, Moat BI, Frajka-Williams E, Rayner D, Meinen CS, Baringer MO, Bryden HL, McCarthy GD (2018) The North Atlantic Ocean is in a State of reduced overturning. *Geophys Res Lett*. <https://doi.org/10.1002/2017GL076350>
- Stommel HM (1965) *The gulf stream: a physical and dynamical description*. University California Press
- Taylor AH, Stephens JA (1998) The North Atlantic oscillation and the latitude of the gulf stream. *Tellus A* 50(1):134–142. <https://doi.org/10.3402/tellusa.v50i1.14517>
- Thiebaut HJ, Zwiers FW (1984) The interpretation and estimation of effective sample size. *J Clim Appl Met* 23:800–811
- Wu Z, Huang NE (2009) Ensemble empirical mode decomposition: a noise-assisted data analysis method. *Adv Adapt Data Anal* 1(1):1–41. <https://doi.org/10.1142/S1793536909000047>
- Wu Z, Huang NE, Long SR, Peng C-K (2007) On the trend, detrending and variability of nonlinear and non-stationary time series. *Proc Nat Acad Sci* 104:14889–14894. <https://doi.org/10.1073/pnas.0701020104>
- Wu L, Cai W, Zhang L, Nakamura H, Timmermann A, Joyce T, McPhaden MJ, Alexander M, Qiu B, Visbeck M, Chang P, Giese B (2012) Enhanced warming over the global subtropical western boundary currents. *Nat Clim Chan* 2:161–166. <https://doi.org/10.1038/nclimate1353>
- Wunsch C, Roemmich D (1985) Is the North Atlantic in sverdrup balance? *J Phys Oceanogr* 15(12):1876–1880
- Yang H, Lohmann G, Wei W, Dima M, Ionita M, Liu J (2016) Intensification and poleward shift of subtropical western boundary currents in a warming climate. *J Geophys Res* 121:4928–4945. <https://doi.org/10.1002/2015JC011513>
- Zhang W, Chai F, Xue H, Oey L-Y (2020) Remote sensing linear trends of the gulf stream from 1993 to 2016. *Ocean Dyn* 70:701–712. <https://doi.org/10.1007/s10236-020-01356-6>
- Zhu C, Liu Z (2020) Weakening Atlantic overturning circulation causes South Atlantic salinity pile-up. *Nat Clim Change* 10:998–1003. <https://doi.org/10.1038/s41558-020-0897-7>

Publisher's Note Springer Nature remains neutral with regard to jurisdictional claims in published maps and institutional affiliations.